

New models of reflection spectra for terrestrial exoplanets: Present and prebiotic Earth orbiting around stars of different spectral types

Manika Singla^{a,b}, Sujan Sengupta^a

^a*Indian Institute of Astrophysics Koramangala Bengaluru 560034 India*

^b*Department of Physics Pondicherry University Kalapet Puducherry 605014 India*

Abstract

In order to recognize a habitable exoplanet from future observed spectra, we present new model reflected spectra and geometric albedo for modern and prebiotic (~ 3.9 Ga) Earth-like exoplanets orbiting within the habitable zone of stars of spectral types F, G, K and M. We compute this for various atmospheric and surface compositions of the planets. Molecules that are potential biosignatures and act as greenhouse agents are incorporated in our model atmosphere. Various combinations of solid and liquid materials such as ocean, coast, land consisting of trees, grass, sand or rocks determine the surface albedo of the planet. Geometric albedo and model reflected spectra for a set of nine potential habitable planets, including Proxima Centauri b, TRAPPIST-1d, Kepler-1649c and Teegarden's Star-b, are also presented. We employ the opacity data derived by using the open-source package *Exo-Transmit* and adopt different atmospheric Temperature-Pressure profiles depending on the properties of the terrestrial exoplanets. The model-reflected spectra are constructed by numerically solving the multiple scattering radiative transfer equations. We verified our model reflected spectra for a few specific cases by comparing with those published by other researchers. We demonstrate that prebiotic Earth-like exoplanets and present Earth-like exoplanets with increased amount of greenhouse gases in their atmospheres scatter more starlight in the optical. We also present the transmission spectra for modern and prebiotic Earth-like exoplanets with cloudy and cloudless

*Corresponding author

Email address: `manika.singla@iiap.res.in` (Manika Singla)

atmospheres.

Keywords: radiative transfer, methods: numerical, planets and satellites: terrestrial planets, atmosphere

1. Introduction

Since the discovery of 51 Pegasi b (Mayor and Queloz, 1995), more than 5000 exoplanets candidates have been discovered using various methods, yet a little has been investigated about their atmospheres. According to Bryson et al. (2020), around half of the Solar-type stars in our Galaxy might host rocky and potentially habitable planets within their habitable zones. But still we are far from finding any exoplanet that may have an ambient environment similar to that of the Earth. We will be a step closer to finding out such planets if we can characterize the atmospheres of terrestrial exoplanets (Selsis, 2004; Morley et al., 2015; Kaltenegger, 2017; Alonso, 2018; Kopparapu et al., 2020; Quanz et al., 2021).

The classical circumstellar habitable zone is defined as the region around a star where the surface temperature of a planet is appropriate for water to exist in liquid state (Huang, 1959, 1960; Whitmire et al., 1991; Kasting et al., 1993; Kopparapu et al., 2013). A few of the planets discovered by the NASA’s *Kepler* space mission, possibly located in the habitable zone of their host stars (Covone et al., 2021), are also of great interest. The recent TESS (Transiting Exoplanet Survey Satellite) discoveries include Super-Earth and Sub-Neptunes orbiting around HD 108236 (G3V), GJ 3929 b, which is a hot Earth sized planet orbiting around M3.5V star (Daylan et al., 2021; Kemmer et al., 2022). Many Earth-like planets, including TOI-700d, which lie in their host star’s habitable zone, discovered by TESS are also important (Kaltenegger et al., 2021). Many potentially habitable exoplanets have also been discovered by RV Spectrographs (Jurgenson et al., 2016; Wildi et al., 2017, and many more).

When stellar radiation is incident on the surface of a planet, parts of it get reflected, absorbed and transmitted depending on the wavelength of the radiation and the angle of incidence of the stellar flux (Seager, 2010; Perryman, 2018). The planetary reflected spectra are generated by the fraction of the incident stellar radiation reflected along our line of sight (Selsis et al., 2008). The interaction of the incident stellar radiation with the matter in the upper atmosphere of the planet introduces signatures of the atmospheric chemical

composition in the reflected spectra. However, when an exoplanet transits across the host star, a tiny portion of the stellar disk is blocked yielding into a reduction in the stellar flux. At the same time, a fraction of star-light passes through the planetary atmosphere, if any, and brings the information on the chemical composition of the planetary atmosphere. This is known as the transmission spectrum (Pallé et al., 2009; Wunderlich et al., 2019). The signatures of the molecules present in the planetary atmosphere are revealed in the absorption features of reflected and transmitted spectra (Tinetti et al., 2013). If a combination of biosignatures, such as oxygen, ozone, water and methane, were detected in the atmosphere of rocky exoplanets in habitable zone, there would be a high possibility that the planet harbours life (Owen, 1980; Sagan et al., 1993; Selsis, 2004; Scharf, 2009; Grenfell et al., 2014; Fujii et al., 2018; Claudi and Alei, 2019).

Previous studies suggested that the potentially habitable planets can orbit stars of F, G, K and M spectral types (Selsis, 2000). According to Kasting et al. (1993), the most potentially habitable planets orbit around late F, G and early K-type main-sequence stars. Stars whose spectral type is earlier than F0 have less than 2 Gyr main sequence lifetimes and hence are very less likely to have planets that can harbour life (Segura et al., 2003). On the other hand, M dwarfs have much less probability of having life supporting planets orbiting around them because their habitable zones are much nearer and narrower and so the planets in the habitable zone are exposed to strong UV radiation and strong flares (Huang, 1959, 1960; Hart, 1979). Also most planets in the inner habitable zone of M dwarfs are tidally locked (Kasting et al., 1993; Segura et al., 2003; Martinez-Rodriguez et al., 2019) and the permanent day or night side of the planet may have hostile environment for life. Nearly 70% of all stars in our Galaxy are M dwarfs and rocky planets orbiting M dwarfs may be the most common in the universe (Henry et al., 2006; Shields et al., 2016; Meadows et al., 2018; Lin and Kaltenegger, 2020; Reylé et al., 2021; Sabotta et al., 2021). Therefore, it is important to include the exoplanets orbiting M dwarfs as well in any investigation and probe.

Exoplanets similar to the prebiotic Earth (~ 3.9 Ga) can also be the potential candidates for supporting life on them. Prebiotic Earth contained no free molecular oxygen but carbon dioxide and nitrogen as the most dominant gases in their atmospheres (Rugheimer et al., 2015). Prevalent oxygenation of the Earth's atmosphere took place somewhere between 2.45 Ga and 2.32 Ga, which is known as the Great Oxidation Event GOE (Holland, 2002; Bekker et al., 2004; Guo et al., 2009). Discovery of the biomarkers in sedimentary

rocks (banded iron formation) with age 2.7 Ga to 2.8 Ga, which are characteristic of photosynthetic cyanobacteria, indicates the appearance of O₂ in the Earth's atmosphere (Brocks et al., 1999). Before this period, life survived through anoxygenic photosynthesis process. The second oxygenation event took place around 0.8 Ga to 0.5 Ga, which is known as Neoproterozoic Oxygenation Event (NOE). During that period, oxygen probably accumulated to the levels that are required for the animal life (Shields-Zhou and Och, 2011; Och and Shields-Zhou, 2012; Hiatt et al., 2020).

About three decades ago, the *Galileo* space mission obtained the reflected spectra of the Earth over a relatively clear sky region of the Pacific Ocean, north of Borneo, which was analysed by Sagan et al. (1993). Previously, many groups have characterized the atmospheres of modern and prebiotic Earth-like exoplanets by calculating reflection and transmission spectra (Ehrenreich et al., 2006; Kaltenegger and Traub, 2009; Kitzmann et al., 2010b; Domagal-Goldman et al., 2014; Wunderlich et al., 2019; Kaltenegger et al., 2020; Lin et al., 2021). Studies have also been done for the Earth-like planets orbiting F, G, K and M stars (Segura et al., 2005; Grenfell et al., 2007; Rugheimer et al., 2013; Rugheimer and Kaltenegger, 2018). An open source radiative transfer model PICASO to calculate the reflected spectra of exoplanets was presented by Batalha et al. (2019). Earth's transmission spectra through lunar eclipse observations were calculated by Pallé et al. (2009, 2010) and Yan et al. (2015).

Previously, Kreidberg and Loeb (2016), Meadows et al. (2016), Dong et al. (2017); Lovis et al. (2017); Luger et al. (2017); Meadows et al. (2018); Lin and Kaltenegger (2020); Scheucher et al. (2020) have characterized the atmosphere for Proxima Centauri b and De Wit et al. (2018); Krissansen-Totton et al. (2018); Moran et al. (2018); Zhang et al. (2018); Lustig-Yaeger et al. (2019); Hori and Ogihara (2020); Lin and Kaltenegger (2020); Turbet et al. (2020); Wunderlich et al. (2020); May et al. (2021) have extensively discussed about TRAPPIST-1 system and in particular the planets TRAPPIST-1d and e. Kaltenegger et al. (2013), on the other hand, modeled the transmission spectra for the planet Kepler-62e. Clouds also play a crucial role in determining reflection and transmission spectra (Kitzmann et al., 2010a,b, 2011a,b; Kawashima and Rugheimer, 2019). Fauchez et al. (2019) demonstrated the effect of clouds and hazes on the transmission spectra of the planets in the habitable zone of TRAPPIST-1, and Pidhorodetska et al. (2020) worked on detectability of molecules through transmission spectroscopy.

In this paper, we present the new synthetic reflected spectra of exoplanets

similar to the modern and prebiotic Earth orbiting around stars of F, G, K and M spectral types. If the atmosphere is optically thick at pressure level much smaller than 10^3 mbar, most of the incident stellar radiation in the optical wavelength region will get absorbed and reflected only by the planetary atmosphere. However, the reflecting properties of the surface play a crucial role in the re-emission of thermal radiation at the infrared wavelength region. The surface albedo of solid or liquid (ocean) surface is also considered, which provides better and realistic model spectra. We also calculate the spectra for nine Earth-like planets that lie in the habitable zone of their host stars.

We also present model transmission spectra for simulated terrestrial exoplanets with atmospheric composition similar to that of the modern as well as prebiotic Earth. For this purpose, we use the publicly available software package `Exo-Transmit`¹ (Kempton et al., 2017). A comparative study of the transmission spectra calculated using the `Exo-Transmit` code and the `TauREx` software package (Waldmann et al., 2015) was presented in Sengupta et al. (2020).

In the next Section, we discuss the methodologies adopted to calculate the reflected spectra and the validation of our results. In particular, numerical methodologies are discussed in Section 2.1 and the absorption and scattering opacities that are employed are described in Section 2.2 and we discuss about Temperature-Pressure profile in Section 2.3. Results are presented in Section 3. The model reflected spectra for both cases - modern and prebiotic Earth-like exoplanets orbiting around stars of F, G, K and M spectral types are presented in Section 3.1 and the model reflected spectra of specific and interesting habitable terrestrial planets are shown in Section 3.2. The model transmission spectra are presented in Section 3.3. Finally we discuss our results with specific conclusions in Section 4.

2. Methodology

2.1. Numerical Methodology

To calculate the reflected spectra, we solved the multiple-scattering radiative transfer equation for diffused reflection and transmission, which for a

¹https://github.com/elizakempton/Exo_Transmit

plane-parallel geometry and azimuthal symmetry, is given by (Chandrasekhar, 1960; Sengupta et al., 2020):

$$\mu \frac{dI(\tau, \mu, \lambda)}{d\tau} = I(\tau, \mu, \lambda) - \frac{\omega}{2} \int_{-1}^1 p(\mu, \mu') I(\tau, \mu', \lambda) d\mu' - \frac{\omega}{4} F(\lambda) e^{-\tau(\lambda)/\mu_0} p(\mu, \mu_0) \quad (1)$$

where $I(\tau, \mu, \lambda)$ is the specific intensity of the diffused radiation field along the direction $\mu = \cos \theta$, θ being the angle between the axis of symmetry and the ray path, ω is the albedo for single scattering, $F(\lambda)$ is the incident stellar flux in the direction $-\mu_0$ and τ is the optical depth such that $d\tau = -\chi dz$, where χ is the total absorption coefficient or extinction coefficient, i.e., the sum of true absorption and absorption due to scattering. In the above equation, $p(\mu, \mu')$ is the scattering phase function that describes the angular distribution of the photons before and after scattering. The scattering phase function depends on the nature of the scatterers. For scattering by atoms and molecules, the angular distribution is described by Rayleigh scattering phase function and is given by Chandrasekhar (1960),

$$p(\mu, \mu') = \frac{3}{4} [1 + \mu^2 \mu'^2 + \frac{1}{2} (1 - \mu^2)(1 - \mu'^2)], \quad (2)$$

where μ and μ' are the cosine of the angle before and after scattering with respect to the normal.

As pointed out by Sengupta et al. (2020), in a scattering medium, the radiation field has two components: the reflected and transmitted intensities, which suffer one or more scattering process, and the directly transmitted flux, which is known as the reduced incident flux (Chandrasekhar, 1960), $\pi F(\lambda) e^{-\tau(\lambda)/\mu_0}$ in the direction $-\mu_0$. So, the reflected and the transmitted intensities that are incorporated through the second term in the right hand side of the above equation, do not include the reduced incident flux, which is described by the third term.

We solved the multiple scattering radiative transfer equations by using the discrete space theory that was developed by Peraiah and Grant (1973) and Peraiah (2002). The numerical code has extensively been used to solve the vector radiative transfer equations to incorporate scattering polarized spectra of brown dwarfs and self-luminous exoplanets (Sengupta and Marley, 2009, 2010, 2016; Marley and Sengupta, 2011; Sengupta, 2016a, 2018). For

the present work, we used the scalar version of the same numerical code by using the following steps:

1. As the vertical atmosphere is heterogeneous with respect to temperature, pressure and optical depth, we divided it into many “shells” of small optical depths. The thickness of each shell is less than or equal to a critical thickness τ_{critical} , which is calculated on the basis of the physical characteristics of the medium. If $\tau \leq \tau_{\text{critical}}$, the reflection and the transmission operators have non-negative elements (Peraiah, 2001). We assume a constant temperature and pressure over each shell, and then integrate the radiation over all the shells.
2. The integration of the transfer equation is performed on the shells, which is a two-dimensional grid bounded by $[r_n, r_{n+1}] \times [\mu_{j-1/2}, \mu_{j+1/2}]$, where, r_n is the radial grid and $\mu_{j+1/2}$ is the angular grid:

$$\mu_{j+1/2} = \sum_{k=1}^j c_k, j = 1, 2, \dots, J \quad (3)$$

Here, c_k are the weights of Gauss-Legendre quadrature formula. We used the plane-parallel approximation by making the shell curvature equal to zero.

3. The Gauss’ quadrature formula is given as (Chandrasekhar, 1960):

$$\int_{-1}^{+1} f(\mu) d\mu = \sum_{j=1}^m a_j f(\mu_j) \quad (4)$$

where μ_1, \dots, μ_m are the zeros of $P_m(\mu)$ and

$$a_j = \frac{1}{P'_m(\mu_j)} \int_{-1}^{+1} \frac{P_m(\mu)}{\mu - \mu_j} d\mu \quad (5)$$

where, $P_m(\mu)$ is known as the Legendre Polynomial of order m . We used the 8-point Gauss’ Quadrature Formula.

4. We obtained the transmission and reflection operators of the shell by comparing these discrete equations with the canonical equations of the interaction principle, which relates the incident and emergent radiation from a medium of given optical depth.

5. Combining all the shells by star algorithm (Peraiah, 2002), we obtained the total radiation field. Star algorithm combines the radiation for two consecutive shells by putting them together and calculating the radiation field as a whole.

The numerical method has been described in detail in Peraiah and Grant (1973), Peraiah (2002), Sengupta and Marley (2009) and Sengupta et al. (2020).

In order to validate our numerical calculations, we compared the model reflected spectra of a terrestrial exoplanet orbiting around a solar-type star with the observed reflected spectra of the Earth (Sagan et al., 1993) obtained by the *Galileo* spacecraft. This is presented in Figure 1. We found an overall good match of the observed low-resolution spectrum with our model spectrum, in particular the dominant water and oxygen bands. The intensity decreases with wavelength in the infrared region because of the nature of input solar spectra and Rayleigh scattering (which is proportional to λ^{-4}).

Figure 2 shows the comparison between the reflected spectra for TRAPPIST-1e as calculated by our model with that calculated by Lin and Kaltenegger (2020). We used the same chemical abundance as in Lin and Kaltenegger (2020) for verification purposes. Temperature-Pressure (T-P) profiles employed for this case were the same as considered by O’Malley-James and Kaltenegger (2019). Here also, the overall nature is the same and the slight variations are due to different opacities used and also they used vertically variable atmospheric abundance, but we used vertically homogenous atmospheric abundance. We also compared our model reflected spectrum for prebiotic Earth-like exoplanets orbiting around Sun-like stars (atmosphere composed of only N₂ and CO₂; Rugheimer et al. 2015) with the model spectrum calculated by S. Ranjan (priv. comm.). Figure 3a demonstrates that the reflection spectrum of prebiotic terrestrial exoplanets calculated by us matches very well with that derived by S. Ranjan. The slight variation is again due to the differences in opacities used in both models. Figure 3b shows the comparison of the geometric albedo, which also matches very well. Here there are no absorption lines because the considered molecules show absorption beyond the limit of the wavelength considered in this work (2.49 μm).

2.2. Absorption and Scattering Opacity

In order to calculate the reflection and the transmission spectra, we calculated the absorption and scattering coefficients of the atmosphere by using

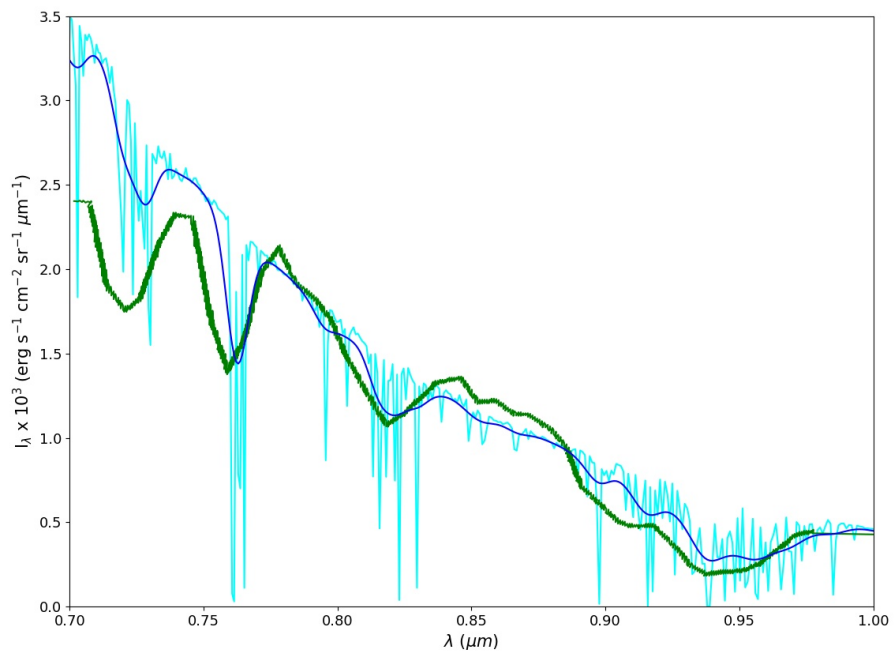


Figure 1: Comparison of the model reflected spectrum (cyan) for an Earth-like exoplanet orbiting around a Sun-like star with the observed reflected spectrum (green) for the Earth obtained by *Galileo* spacecraft (Sagan et al., 1993). Blue color represents the model spectra at a spectral resolution same as NIMS in *Galileo* spacecraft.

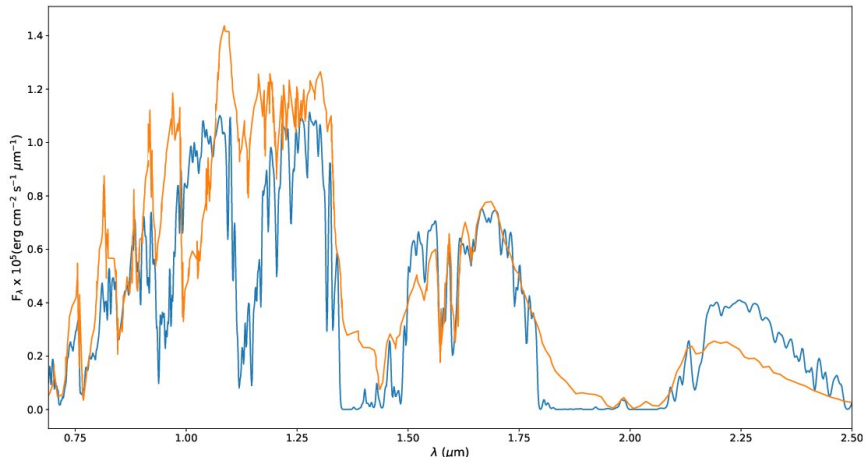


Figure 2: Comparison of the modeled reflected spectra for TRAPPIST-1e (blue) with the spectra calculated by (Lin and Kaltenegger, 2020) (orange).

the `Exo-Transmit` software package (Kempton et al., 2017). In this package, the opacities for 30 molecular and atomic species on a fixed temperature-pressure-wavelength grid are tabulated. The wavelength grid ranges from 0.3 to 30 μm at low spectral resolution of $\mathcal{R} \approx 1000$. The temperature and pressure range at which the absorption and scattering coefficients were calculated for each wavelength were 100–3000 K and 10^{-6} – 10^6 mbar respectively. The opacities were derived by using the line lists given by Lupu et al. (2014). The gas opacities were adopted from the widely used database of Freedman et al. (2008, 2014). The individual opacity sources are the atomic and molecular opacity weighted by their abundances and the total Rayleigh scattering opacity. Since the Earth’s atmosphere is sufficiently cool, we neglected the collision induced absorption of hydrogen. We adopted the molecular abundances of the present Earth (Sagan et al., 1993) as described in Table 1. For the prebiotic Earth-like exoplanets, we considered a carbon dioxide dominated atmosphere with the molecular abundance as 10% CO_2 , trace amounts of CH_4 and the remaining N_2 as considered by Kaltenegger et al. (2007). The atmospheric abundances of Proxima Centauri b, Kepler-442b, Kepler-62e, Kepler-22b, Kepler-1649c, TOI-400d, Teegarden’s Star b, Trappist-1d and TRAPPIST-1e were considered to be the same as that of the present Earth.

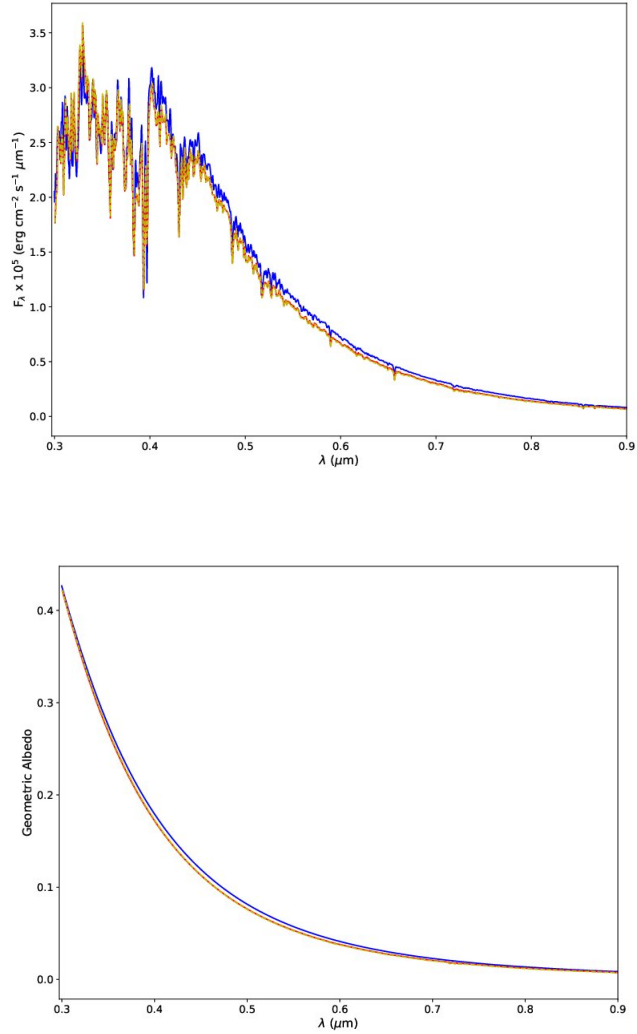


Figure 3: (a) Comparison of our model reflected spectrum (blue) calculated by using opacity from `Exo-Transmit` package and observed atmospheric T-P profile of the Earth with the theoretical spectrum (dashed yellow) provided by S. Ranjan (priv. comm.) as well as with the spectrum calculated by our radiative transfer code using the same opacity and T-P profile as used by S. Ranjan (red) for a prebiotic Earth-like exoplanet orbiting around a solar-type of star. Yellow and red curves are essentially the same. (b) Comparison of the geometric albedo for the above three cases.

Molecule	Abundance (volume mixing ratio)
N ₂	0.78
O ₂	0.21
H ₂ O	0.03 - 0.001
Ar	9×10^{-3}
CO ₂	3.5×10^{-4}
CH ₄	1.6×10^{-6}
N ₂ O	3×10^{-7}
O ₃	$10^{-7} - 10^{-8}$

Table 1: Molecular abundance for the Earth’s atmosphere (Sagan et al., 1993).

For the verification purpose for TRAPPIST-1e, the atmospheric abundance and T-P profile were adopted following O’Malley-James and Kaltenegger (2019). The molecular abundances were incorporated in the equation of states file in the `Exo-Transmit` package, in which pressure and temperature were also included for the atmospheric layers.

2.3. Temperature-Pressure profile

For the terrestrial exoplanets, the internal temperature is negligible as compared to the irradiated temperature. Thus the incident stellar flux at the top-most layer of the atmosphere and the molecules present in the atmosphere determine the Temperature-Pressure (T - P) profile of the terrestrial exoplanets.

Most of the stellar radiation gets reflected from the upper layers of the planetary atmosphere. So, the temperature structure of the outer layers of the atmosphere mostly determines the reflected spectra. In the case of transmission spectra also, the lower atmosphere cannot be probed for most of the wavelengths (Kaltenegger and Traub, 2009). Hence, for the present Earth-like exoplanets orbiting around stars of F, G, K and M spectral types, we adopted the Earth’s atmospheric T - P profile (NOAA NASA US Air Force, 1976), which is shown in Figure 4. As we go upwards from the solid surface of the Earth, the temperature decreases continuously with the decrease in pressure, thus following the ideal gas law in the tropospheric region. This region extends roughly about 9 km at the poles and 17 km at the equator (Caballero et al., 2022). We will roughly consider the height of the tropopause equal to 11 km for our calculations. In the stratospheric region, which extends about 35 km above the tropopause, the temperature increases with

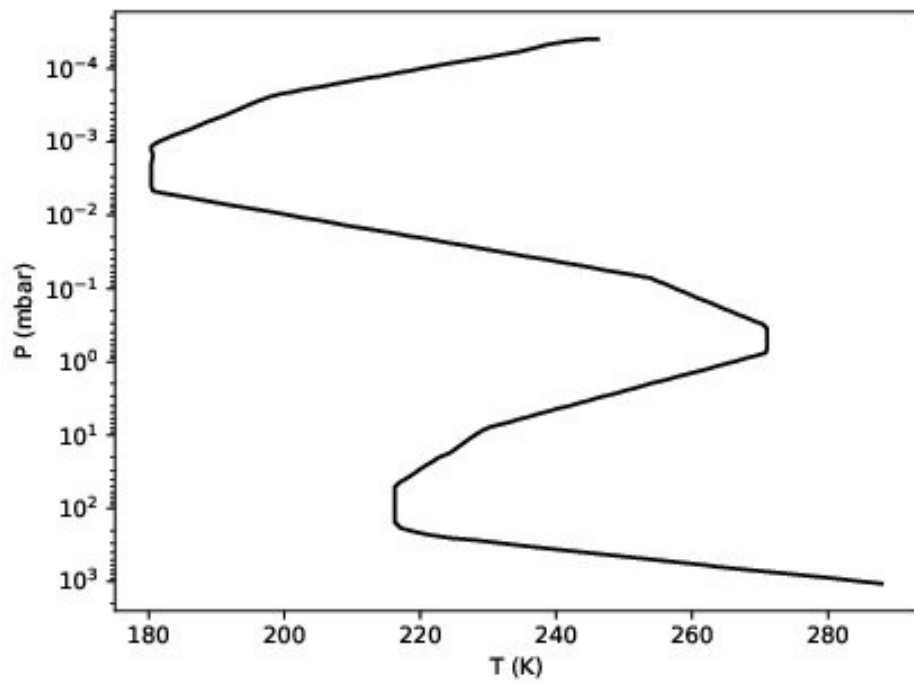


Figure 4: Atmospheric Temperature-Pressure (T-P) profile for the present Earth (NOAA NASA US Air Force, 1976).

the decrease in pressure due to the presence of ozone gas , which absorbs the ultraviolet radiation. This is known as the temperature inversion (NOAA NASA US Air Force, 1976). The T - P profile for the atmospheres of early Earth-like exoplanets is taken the same as considered in Kaltenegger et al. (2007) for Epoch 0 (3.9 Ga).

3. Results and Analysis

3.1. The Reflection Spectra

While orbiting its host star, an exoplanet reflects part of the starlight along our line of sight. We observe the maximum reflected radiation when the planet is almost at full phase or at zero degree phase angle, i.e, just before or after the secondary eclipse position.

In the present investigation, we considered terrestrial planets around stars of three sub-classes 0, 2 and 5 of F, G, K and M spectral types so that late to early stages of each spectral type are included. All the stars were considered to be of main sequence dwarfs of luminosity class V. The input stellar fluxes at the surface of the planets orbiting within the habitable zone of their host stars are shown in Figure 5. The fluxes at the stellar surface for F, G and K spectral types were obtained from ESO library (Pickles, 1998). For the M spectral type, the stellar fluxes were obtained from PHOENIX model (Husser et al., 2013) generated through publicly available code petitRADTRANS (Mollière et al., 2019). The equilibrium temperatures of the planets were assumed to be same as that of the present Earth, i.e. 288 K.

3.1.1. Reflected spectra for present Earth-like exoplanets

We calculated the reflected spectra by solving the multiple-scattering radiative transfer equation for plane-parallel stratification (equation (1)). To estimate the surface Bond albedo of the rocky planets, we considered few different types of surfaces with the compositions given in Table 2.

The surface composition of the present Earth is 70% ocean, 2% coast and 28% land, which is divided into 30% grass, 30% trees, 9% granite, 9% basalt, 15% snow and 7% sand (Kaltenegger et al., 2007). And the surface composition for prebiotic Earth is 70% ocean, 2% coast and 28% land. The land surface consists of 35% basalt, 40% granite, 15% snow and 10% sand with no land vegetation (Kaltenegger et al., 2007; Rugheimer and Kaltenegger, 2018). In the sixth scenario, no solid or liquid surface exists, which means that the atmosphere of the planet is so optically thick, that the incoming

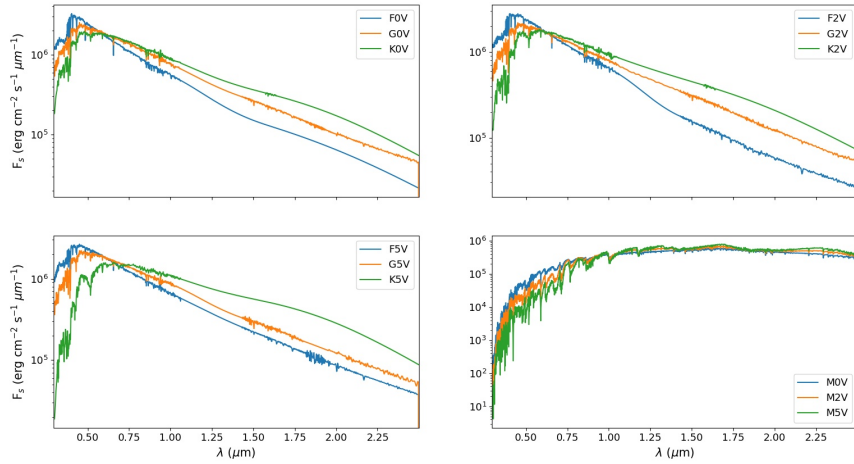


Figure 5: Input stellar flux at the surface of a habitable terrestrial planet orbiting around stars of various sub-classes of F, G, K and M spectral classes.

S.No.	Surface composition	Surface albedo
1	Ocean cover (100%)	0.06
2	Ocean (50%), Trees and grass (50%)	0.1
3	Present Earth-like	0.14
4	Prebiotic Earth-like	0.16
5	Ocean (83%) and snow (17%)	0.2
6	No solid or liquid surface	0

Table 2: Surface Bond albedo for various surface compositions considered in our calculations for the modeled reflected spectra.

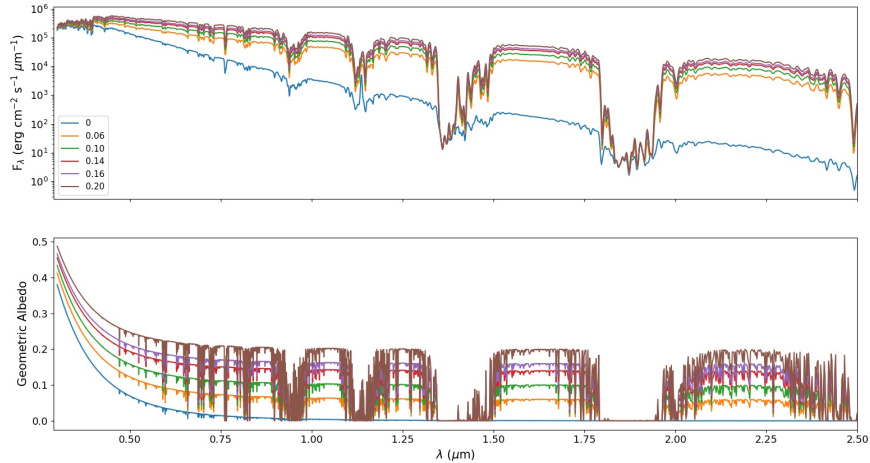


Figure 6: (a) Reflected spectra for present Earth-like exoplanets orbiting around solar type star for different surface compositions (or different surface albedo). Blue line represents the spectra with zero surface albedo, orange line is for 100% ocean cover (surface albedo = 0.06), green line is for 50% ocean cover and the remaining 50% covered with trees and grass (0.1), red line is for present Earth-like surface composition (0.14), purple line is for prebiotic Earth-like surface composition (0.16) and brown line represents the spectra for 83% ocean and the remaining is snow (0.2). (b) Geometric albedo for the same.

stellar radiation gets reflected only from the atmosphere and it does not reach up to the surface. Hence, in this case, surface albedo does not affect the reflected spectra or the geometric albedo. Zero surface albedo may also mean the gaseous planets, which is beyond the scope of this work.

We calculated the surface Bond albedo by weighted sum of all the components' albedo. And the weight factors are the respective fractions of the planetary surface coverage. The reflected spectra for present Earth-like exoplanets orbiting around solar type of star for different surface albedo are shown in Figure 6. Reflected flux increases with the increase in the surface albedo and it is steeper than the input stellar flux because of Rayleigh scattering. The effect of surface albedo on the geometric albedo for the present Earth-like exoplanets is shown in Figure 6b. We can see that geometric albedo increases with the increase in surface albedo. However, it decreases with the wavelength because Rayleigh scattering is not significant at longer wavelength region.

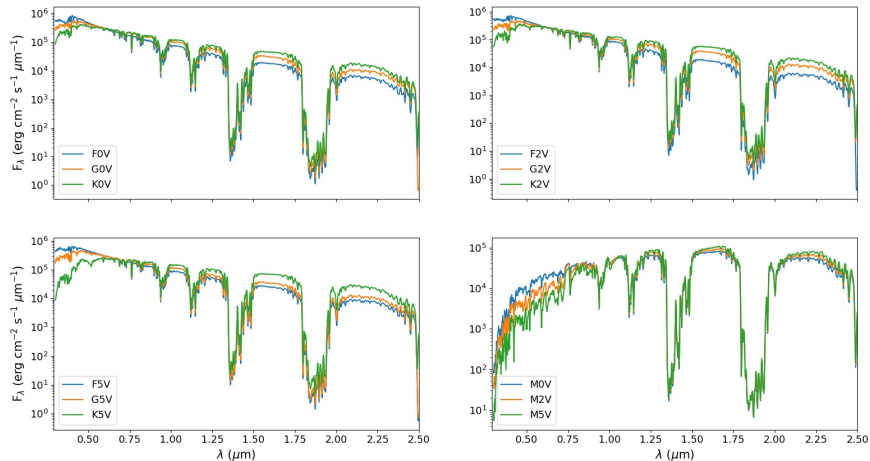


Figure 7: Reflected spectra for present Earth-like exoplanets orbiting around stars of spectral types F, G, K and M.

The reflected spectra for the present Earth-like exoplanets orbiting around stars of F, G, K and M spectral types are shown in Figure 7. The absorption lines of H_2O ($0.72 \mu\text{m}$, $0.82 \mu\text{m}$, $0.94 \mu\text{m}$, $1.10 \mu\text{m}$ and $1.87 \mu\text{m}$), O_2 ($0.63 \mu\text{m}$, $0.69 \mu\text{m}$, $0.76 \mu\text{m}$) and CH_4 ($1.60 \mu\text{m}$) are also shown in this figure. The flux decreases with the increase in the wavelength in the infrared region. This is because of two reasons: firstly, the input stellar flux also decreases with the increase in wavelength in infrared and secondly Rayleigh scattering dominates in the shorter wavelength region (Ityaksov et al., 2008). The reflected spectra has the planetary atmospheric features as well as the stellar atmospheric features.

In the present study, we ignored the effect of strong stellar ultra-violet irradiation that may alter the planetary environment by dissociating water molecules and energy limited hydrogen loss (Sanz-Forcada et al., 2011; Sengupta, 2016b). Presence of sufficient initial water content at the planetary surface may still avoid the planet to become parched under such situation. However, since most of the planets in the habitable zone of M dwarfs are tidally locked, the presence of an Earth-like planet is rare (Martinez-Rodriguez et al., 2019).

In order to investigate the effect of various greenhouse gases on the geo-

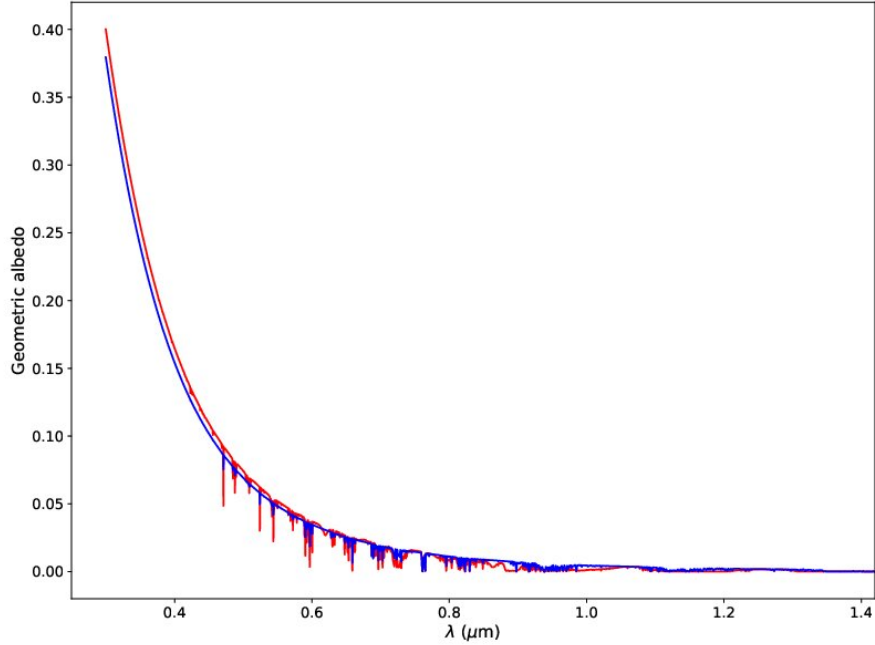


Figure 8: Geometric albedo for present Earth-like exoplanets with Earth-like atmospheric composition (blue) versus geometric albedo with increased abundances of greenhouse gases (red).

metric albedo, we increased the abundance of CO_2 by two orders in magnitude, CH_4 by four orders in magnitude and H_2O by one order in magnitude. This increase is compensated by altering the abundance of N_2 . The geometric albedo of the present Earth-like exoplanets with increased abundances of atmospheric greenhouse gases is presented in Figure 8. We found that the geometric albedo increases slightly in the shorter wavelength region because of the increase in Rayleigh scattering. However, the scattering could have drastic effect in the thermal re-emission at the near and far infrared wavelength region and hence in determining the surface temperature of the planet by an increased greenhouse effect.

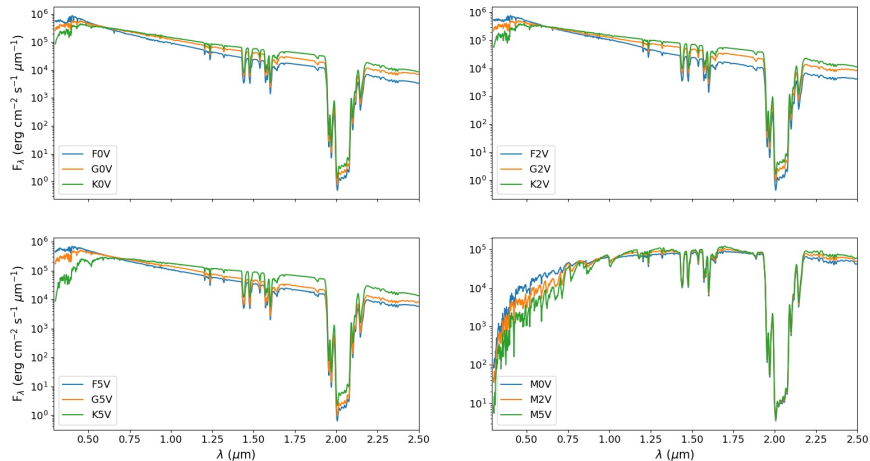


Figure 9: Same as Figure 7 but for early Earth-like exoplanets.

3.1.2. Early Earth-like exoplanets

The reflected spectra for the prebiotic Earth orbiting around stars of F, G, K and M spectral types are presented in the Figure 9. And the geometric albedo (for surface albedo 0.16) is presented in Figure 10. We see very less absorption lines because only N_2 , CO_2 and CH_4 were considered in the atmospheric composition for the prebiotic Earth. The absorption lines of CO_2 ($1.4 \mu m$, $1.6 \mu m$ and $2 \mu m$) and CH_4 ($1.66 \mu m$) can be seen. The overall nature of spectra remains the same as that for the modern Earth case.

A comparison between the geometric albedo for present and prebiotic Earth with zero surface albedo is shown in the Figure 11. Prebiotic Earth-like exoplanets scatter more starlight as compared to the present Earth-like exoplanets because of greater abundances of greenhouse gases (mainly CO_2). The absorption lines for the present Earth are also shown in this figure.

3.2. Reflected spectra of known terrestrial exoplanets

We also present the reflected spectra for some of the well known habitable planets such as Kepler-442b, Kepler-62e, Kepler-22b, TOI-700d, Kepler-1649c, Teegarden's Star b, Proxima Centauri b, TRAPPIST-1d and TRAPPIST-1e. These planets orbit stars of G, K and M spectral types. Their radii are in the range of $0.7 R_{\oplus}$ and $2.4 R_{\oplus}$. These planets lie in the habitable planets catalog in Hill et al. (2022). Although very little is known about their

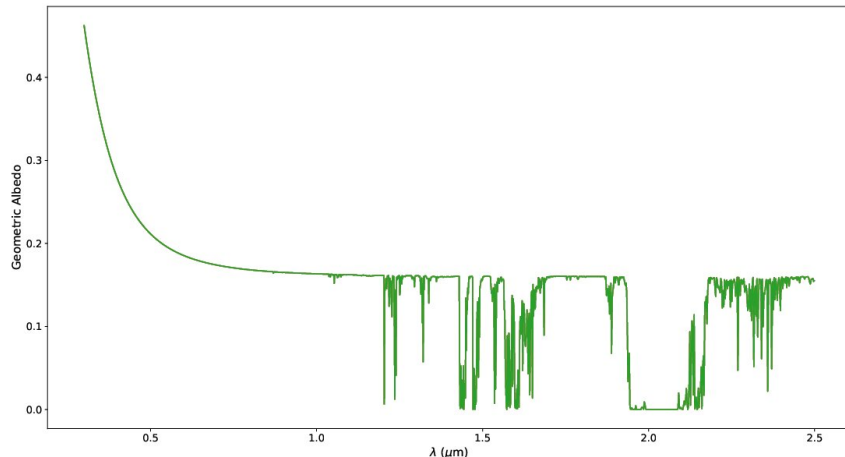


Figure 10: Geometric albedo for early Earth-like planets for surface for surface albedo = 0.16.

atmospheres at present, we expect them to have Earth-like atmospheric compositions with favourable temperature due to greenhouse effect. The input stellar flux at the surface of Kepler-442b, Kepler-62e and Kepler-22b were calculated by taking the stellar flux from Pickles (1998). We used PHOENIX model spectra for the cases of TOI-700d, Kepler-1649c and Teegarden’s Star b. For Proxima Centauri b, the stellar flux is taken from (Lin and Kaltenegger, 2020) and for TRAPPIST-1d and TRAPPIST-1e, we used the spectra from Burgasser et al. (2015).

Their equilibrium temperature T_{eq} can be derived from the relationship given in equation 6 (Seager, 2010). The temperature at the bottom of the atmosphere (or surface temperature) with greenhouse effect is given by equation 7 (De Pater and Lissauer, 2015).

$$T_{\text{eq}}^4 = (1 - A) \frac{R_s^2}{2a} T_{\text{eff}}^4 \quad (6)$$

$$T_{\text{surf}}^4 = T_{\text{eq}}^4 \left(1 + \frac{3}{4} \tau_g\right) \quad (7)$$

In equations 6 and 7, A is the Bond albedo, R_s is the radius of the host star, a is the orbital distance, T_{eff} is the effective temperature of the host

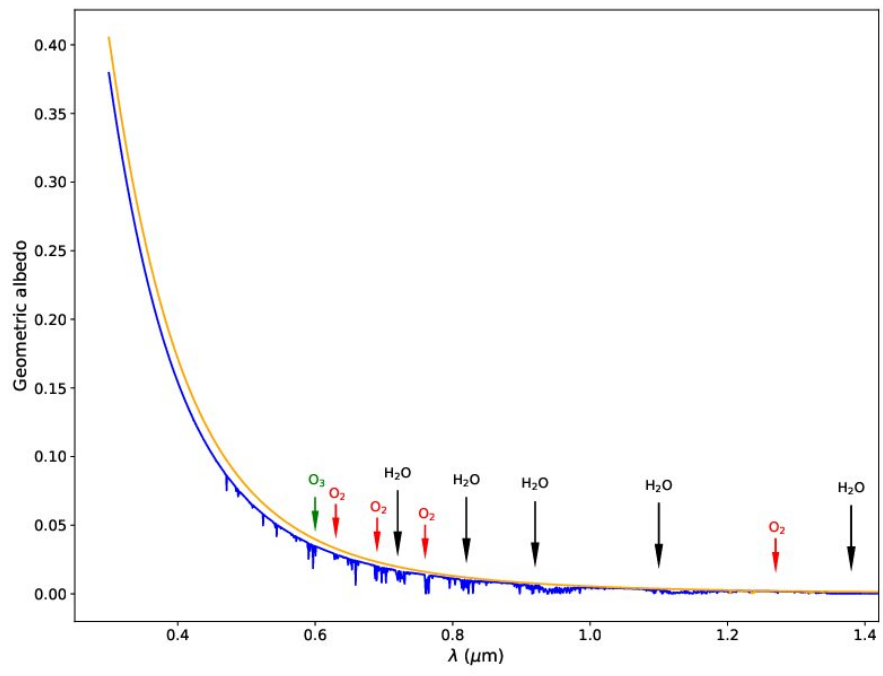


Figure 11: Geometric albedo for present (blue) and prebiotic (orange) Earth-like exoplanets for zero surface albedo.

star, T_{surf} is the temperature at the surface of the planet with greenhouse effect and τ_g is the optical depth of the atmosphere at infrared wavelengths. We assumed it to be same as that for the Earth, i.e. ~ 0.83 . The surface temperature should not be less than 273 K for the planet to be habitable ($T_{\text{surf,min}} \approx 273$ K). And from equation 7, the minimum equilibrium temperature or the temperature at the top of the atmosphere ($T_{\text{eq,min}}$) is about 242 K.

3.2.1. *Kepler-442b*

It is an Earth-like exoplanet orbiting its host star (K5V) within the habitable zone and about 366 pc away from the Earth. It is among all the detected rocky planets that is most similar to the Earth and has a very high habitability index value (Torres et al., 2015; Kane et al., 2016; Rodríguez-Mozos and Moya, 2017). This planet receives an incident stellar flux that is 0.9 times of the flux received by the Earth (Torres et al., 2015; Armstrong et al., 2016; Rodríguez-Mozos and Moya, 2017; Barbato et al., 2018). It is a promising candidate for search of biosignatures as K-type of stars maintain favourable circumstellar conditions for habitability (Cuntz and Guinan, 2016). Its density is very similar to the Earth and mean surface gravity is ~ 12.5 m/s², slightly higher than that of the Earth. According to Arney (2019), K-type stars present an advantage for the detectability of biosignatures. One of the reasons is that K dwarfs offer extended photochemical lifetime of methane as compared to G types stars. And the other reason is better signal-to-noise ratio (S/N) of K dwarfs than G dwarfs, due to which oxygen and methane can be strongly observed. We calculate the T - P profile by the following method:

1. For tropospheric region (up to 11 km), $T = -mh + T_{\text{surf}}$ where m is the adiabatic lapse rate.

$$T_{\text{surf,min}} \approx 273 \text{ K}; \text{ For } h=11 \text{ km, } T \approx 242 \text{ K}; m = 2.83 \text{ K/km}$$

$$T_{\text{surf,max}} \approx 290.1 \text{ K}; \text{ For } h=11 \text{ km, } T \approx 257 \text{ K}; m = 3 \text{ K/km}$$

$$T_1 = -2.83h + 273; T_2 = -3h + 290.1 \quad (8)$$

2. For Stratospheric region and above, $T_1 \approx 242$ K; $T_2 \approx 257$ K.

Similarly, we calculated the T - P profile for all the other planets by calculating their adiabatic lapse rates. The possible range of T - P profile for Kepler-442b is shown in Figure 12 and the temperature can lie anywhere in this range. The maximum value of Bond albedo (A_{max}), temperature at

Planet	$T_{\text{eq,max}}$ (K)	$T_{\text{surf,max}}$ (K)	$A_{\text{Bond,max}}$	$R_p^{[1]}$ (R_{\oplus})	$M_p^{[1]}$ (M_{\oplus})	$a^{[1]}$ (au)	ESI ^[2]
Kepler-442b	257	290	0.216	1.34	2.36	0.409	0.84
Kepler-62e	291	328	0.52	1.61	36	0.427	–
Kepler-22b	286	323	0.486	2.33	36	0.849	–
TOI-700d	269	304	0.347	1.144	1.57	0.1633	0.93
Kepler-1649c	296	334	0.55	1.06	1.2	0.0649	0.90
Teegarden b	289	326	0.51	1.02*	1.05	0.0252	0.95
Proxima b	258	292	0.2289	1.08*	1.27	0.0485	0.87
TRAPPIST-1d	286	323	0.49	0.788	0.388	0.0223	0.90
TRAPPIST-1e	250	282	0.12	0.92	0.692	0.0292	0.85

Table 3: $T_{\text{eq,max}}$ is the maximum temperature at the top of the atmosphere of the planet and $T_{\text{surf,max}}$ is the maximum temperature at the bottom of the atmosphere after considering greenhouse effect. A_{max} is the maximum possible Bond albedo, ESI is the Earth similarity index, R_p and M_p are the radius and mass of the planet and a is the orbital separation. [1]<https://exoplanets.nasa.gov/exoplanet-catalog/> [2]<https://phl.upr.edu/projects/earth-similarity-index-esi>
*estimate value

the top of the atmosphere (T_{eq}) and temperature at the bottom of the atmosphere including green-house effect (T_{surf}) were calculated in the same ways and are shown in Table 3. The atmospheric abundance was assumed to be the same as that of the Earth and shown in Table 1. We calculated the reflected spectra for the two T - P profiles and found that the spectra does not alter with the variation in T - P profile within the given range. The reflected spectra for the planet Kepler-442b for various surface compositions i.e. different surface albedos is shown in the Figure 12.

Figure 12 also shows the geometric albedo of Kepler-442b for different surface compositions of the planet. We note that the geometric albedo increases significantly with the increase in the surface Bond albedo or we can say that the surface albedo considerably affects the geometric albedo. This is because the surface also contributes in the total reflectivity of the planet. For example, for the zero surface albedo case, the geometric albedo is the least. And it is maximum for the present Earth-like surface components (0.14 surface albedo).

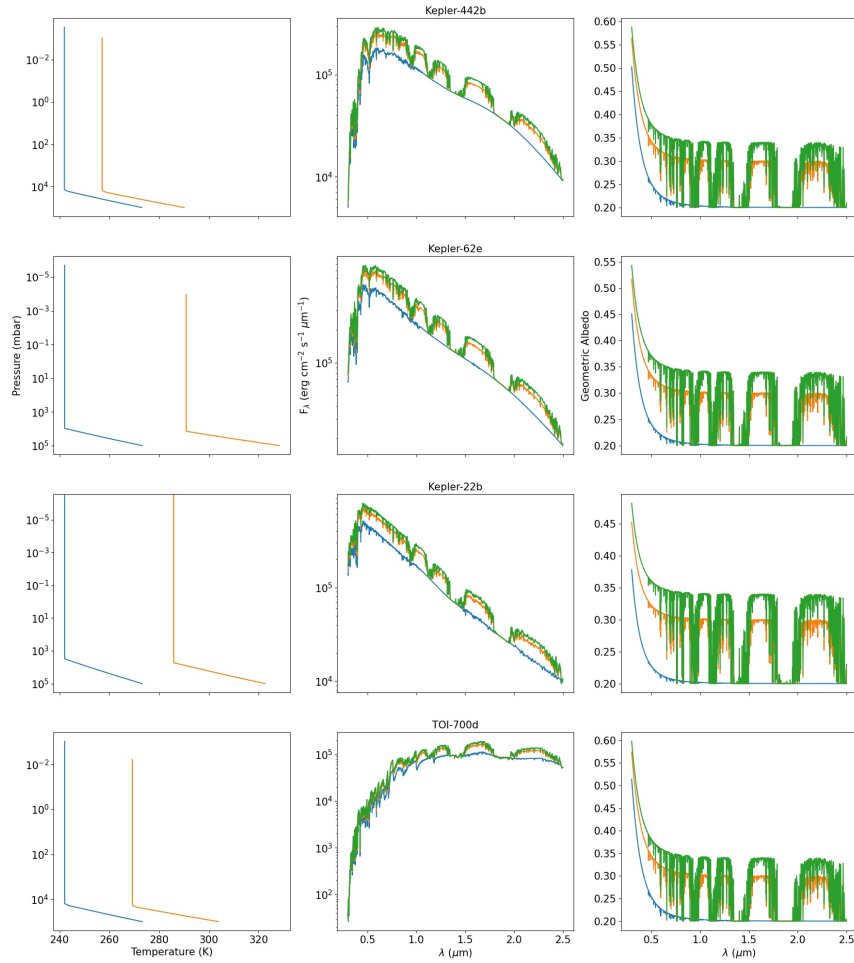


Figure 12: (a) Possible range of T - P profile; Effect of the surface albedo on (b) the reflected spectra; and (c) geometric albedo for Kepler-442b, Kepler-62e, Kepler-22b and TOI-700d. Green curve is for the Earth-like surface composition (surface albedo = 0.14), orange for 50% ocean and 50% land consisting of trees and grass only (0.1) and blue for zero surface albedo (i.e., no solid/liquid surface)

3.2.2. *Kepler-62e*

Kepler-62e also orbits within the classical habitable zone of the host star (K2V) and the orbital period is about 122 days (Borucki et al., 2013; Kaltenegger et al., 2013; Torres et al., 2015; Armstrong et al., 2016; Kane et al., 2016). The possible T - P profile was calculated in the same way as in the case of Kepler-442b and is presented in Figure 12. The temperature and pressure can be anywhere between these limits.

The reflected spectra and the geometric albedo for Kepler-62e are also shown in Figure 12 for various surface compositions. It is highest for Earth-like surface composition (surface albedo 0.14) and lowest for no surface albedo at all. The green curve is for 50% ocean cover and the remaining covered with trees and grass. As the ocean cover is reduced from 70% to 50% by increasing the land cover, the geometric albedo decreases.

3.2.3. *Kepler-22b*

Kepler-22b is a super-Earth orbiting a G5V star, which is about 194.7 pc away from Earth. This planet is also orbiting within the habitable zone of the host star (Borucki et al., 2012; Neubauer et al., 2012; Torres et al., 2015; Kane et al., 2016). It is the first detected Earth-like exoplanet in the habitable zone of a solar-type star.

The atmospheric T - P profile used to calculate the reflected spectra of the planet is shown in Figure 12. It is also calculated by assuming the atmosphere of the planet in hydrostatic equilibrium and considering greenhouse effect.

The effect of the surface Bond albedo (derived from the surface compositions) on the reflected spectra and the variation of the geometric albedo are also shown in Figure 12.

3.2.4. *TOI-700d*

It is TESS's first Earth-size exoplanet, which lies in the habitable zone of its host star TOI-700 (M dwarf). The planet is expected to be tidally locked as its eccentricity is close to zero (Gilbert et al., 2020; Rodriguez et al., 2020; Suissa et al., 2020; Kaltenegger et al., 2021). It receives about 86% of the insolation that the Earth receives (Gilbert et al., 2020). The possible range of the atmospheric T - P profile for this planet is shown in Figure 12. The reflected spectra and the geometric albedo are also shown in this figure.

3.2.5. *Kepler-1649c*

This is an Earth-size planet lying in the habitable zone of its host star , which is of M5V spectral type. It is located at a distance of about 92 pc from the Earth (Vanderburg et al., 2020; Kane et al., 2020; Gvalani, 2022). The T - P profile, the reflected spectra and the geometric albedo are presented in Figure 13.

3.2.6. *Teegarden's Star b*

Teegarden's Star was discovered by Teegarden et al. (2003) and it is at a distance of 3.831 pc and of spectral type M7V (Alonso-Floriano et al., 2015). It has two planets Teegarden's Star b and c. Both of them are super Earths but Teegarden b is the most Earth-like planet or maximum ESI value (see Table 3), discovered till now (Wandel and Tal-Or, 2019; Zechmeister et al., 2019). This planet lies within the habitable zone and it is tidally locked. The T-P profile range, reflected spectra and the geometric albedo are presented in Figure 13.

3.2.7. *Proxima Centauri b*

Proxima Centauri b is a rocky planet that orbits within the habitable zone of our nearest neighbour Proxima Centauri (M5V), which receives about 65% of the total flux that our Earth receives from the Sun (Anglada-Escudé et al., 2016; Garraffo et al., 2016; Turbet et al., 2016; Ribas et al., 2017; Meadows et al., 2018; Lin and Kaltenegger, 2020; Galuzzo et al., 2021).

We modeled the reflected spectra of Proxima Centauri b by using the stellar flux presented by Lin and Kaltenegger (2020). The T - P profile (derived in the same way) for the atmosphere of Proxima Centauri b is shown in Figure 13 where a range is given. The reflected spectra and the geometric albedo for Proxima Centauri b are shown in Figure 13 for various surface Bond albedo determined by different surface compositions. Here also, it is maximum for Earth-like surface composition and minimum for no surface albedo.

3.2.8. *TRAPPIST-1d and e*

TRAPPIST-1 is another M dwarf of spectral type M8V , which is about 12 pc away from us, hosts seven rocky planets out of which, three are in the habitable zone of the star (Gillon et al., 2016; Burgasser and Mamajek, 2017; Gillon et al., 2017; O'Malley-James and Kaltenegger, 2019; Lin and Kaltenegger, 2020). TRAPPIST-1e is most likely to have habitable surface conditions, as it receives about $\sim 66\%$ of stellar radiation that the Earth

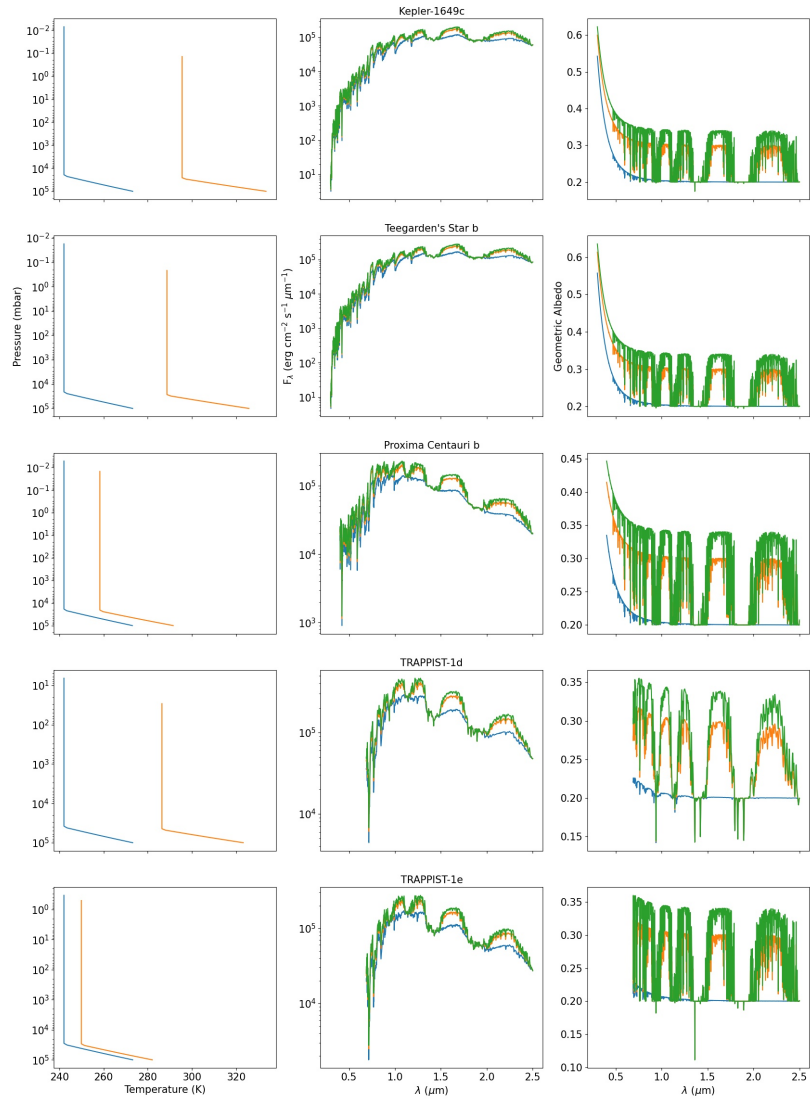


Figure 13: Same as Figure 12 but for Kepler-1649c, Teegarden's Star b, Proxima Centauri b, TRAPPIST-1d and TRAPPIST-1e.

receives from the Sun and needs very little greenhouse effect to have a surface temperature such that water can exist in liquid state (Kopparapu et al., 2013; Wolf, 2017, 2018; Fauchez et al., 2020). Also, TRAPPIST-1e is quite similar in size to the Earth. On the other hand, TRAPPIST-1d has a very high ESI value of 0.9 (see Table 3). So it becomes important to model both the planets.

The T - P profile, the reflected spectra and the geometric albedo are presented in Figure 13 for both the cases. The reflected spectra and the geometric albedo were calculated for various surface materials. As the surface albedo increases, the reflected flux increases because the surface also contributes to the reflected flux. The geometric albedo is decreasing with the increase in wavelength because scattering becomes negligible at longer wavelengths. Also it decreases significantly with the decrease in the surface Bond albedo. For the zero surface albedo case, all the radiation is reflected only from the atmosphere.

3.2.9. Comparisons

The input stellar flux at the surface of the above planets is shown in Figure 14a. The reflected spectra for these planets for Earth-like surface albedo are shown in Figure 14b and the geometric albedo is shown in the Figure 14c. We can see that the reflected spectra follows the input stellar spectra in the visible wavelength region. The geometric albedo is highest for Kepler-22b and lowest for TRAPPIST-1e in the infrared. But in the optical, it is highest for the case of Teegarden’s Star b and lowest for Kepler-22b.

The geometric albedo in the optical region is not estimated for any of the planets around TRAPPIST-1 because it is a late M dwarf whose effective temperature is about 2400K. Its blackbody spectra peak lies at around $1\ \mu\text{m}$ and thus the flux in the optical is very less in magnitude as compared to the flux in NIR. The nature of geometric albedo depends on the absorption and scattering co-efficients of the planetary atmosphere or the T - P profile and the atmospheric composition of the corresponding planet.

3.3. The Transmission Spectra

When an exoplanet transits in front of its host star, it blocks some of the starlight along our line of sight resulting into a reduction in the observed stellar flux. During the transit, a fraction of the stellar radiation passes through the planetary atmosphere providing signatures of the gases present there. The stellar radiation that suffers absorption and scattering in the

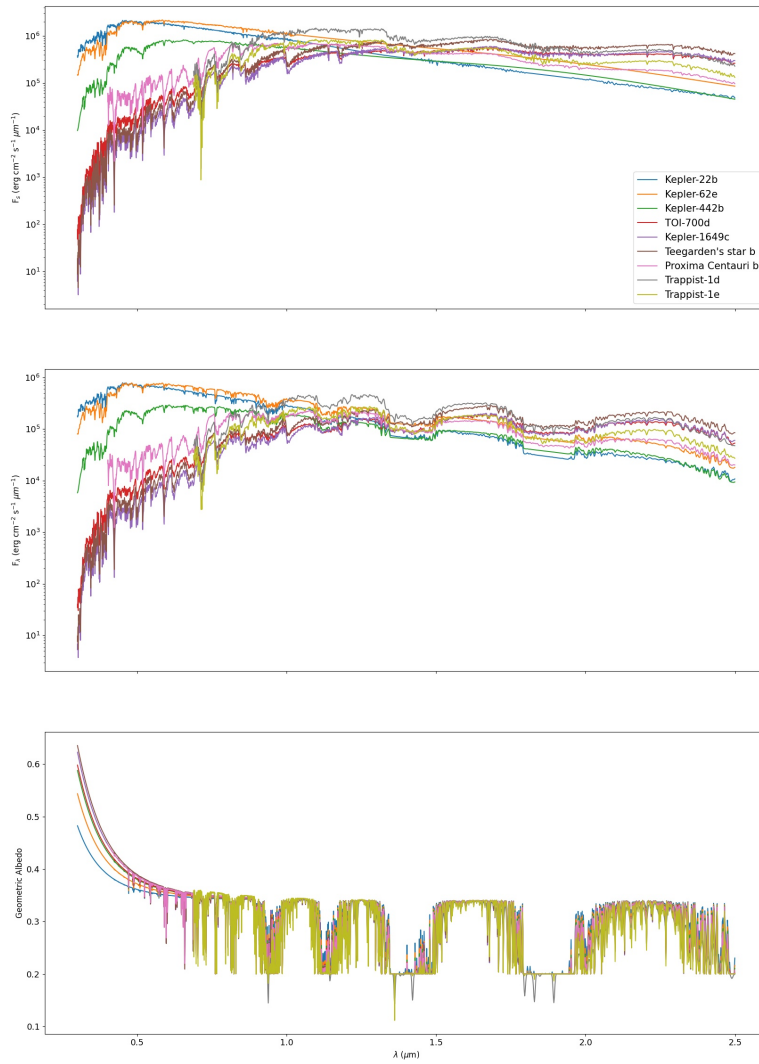


Figure 14: Comparison of the (a) input stellar flux, (b) reflected spectra and (c) geometric albedo for the nine planets in habitable zone.

atmosphere of the planet is known as the transmission or transit spectra. The transmission spectra is usually presented by a wavelength dependent quantity called the transmission or transit depth.

3.3.1. Transit Depth

Transit depth is the ratio between the stellar flux obtained with and without transit. It can be expressed as

$$D = 1 - \frac{F_{trans}}{F_{star}} \quad (9)$$

where F_{trans} is the stellar flux obtained during the planetary transit epoch and F_{star} is the unblocked stellar flux or the stellar flux during the out of transit epoch. F_{trans} can be written as (Kempton et al., 2017; Sengupta et al., 2020):

$$F_{trans} = [1 - (\frac{R_{pl,atm}}{R_{star}})^2]F_{star} + F_{atm} \quad (10)$$

where, $R_{pl,atm}$ is the radius of the planet including its atmosphere and R_{star} is the radius of the star, F_{atm} is the stellar flux, which gets transmitted through the planetary atmosphere along the line of sight. Transit depth corresponds to the ratio between the planetary radius $R_{pl,atm}$ and the stellar radius R_{star} .

In order to calculate F_{atm} , we used Beer-Bouguer-Lambert's law given by:

$$I(\lambda) = I_0(\lambda)e^{-\tau_\lambda/\mu_0} \quad (11)$$

where $I(\lambda)$ is the intensity of the transmitted stellar radiation through the planetary atmosphere and $I_0(\lambda)$ is the intensity of the incident stellar radiation on the planet. In the above equation, τ_λ is the optical depth along the ray path and μ_0 is the cosine of the angle between the direction of the incident radiation and the normal. The expression for the optical depth along the line of sight ($\tau(\lambda, z)$) is given by:

$$\tau(\lambda, z) = 2 \int_0^{l(z)} \chi(\lambda, z)\rho(z)dl \quad (12)$$

where $\chi(\lambda, z)$ is the extinction coefficient, which is the sum of the absorption coefficient and the scattering coefficient, $\rho(z)$ is the density of the planetary atmosphere, z is the height of the atmosphere from the planetary surface, l

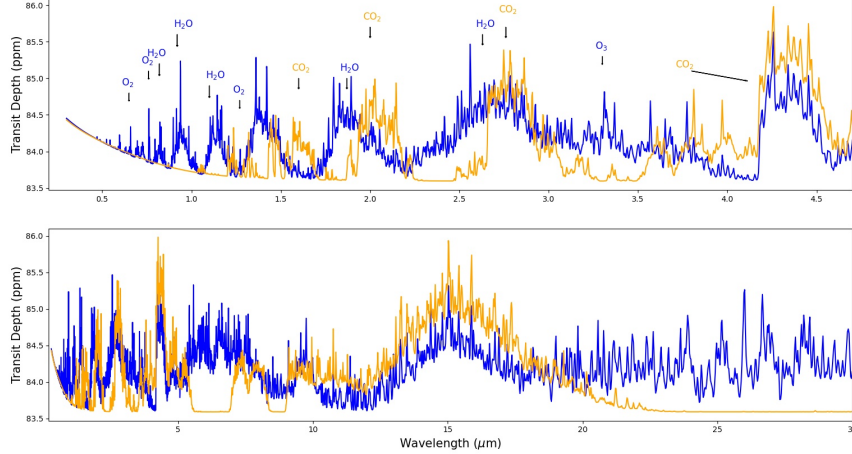


Figure 15: Transmission spectra of present (blue) and early (orange) Earth-like exoplanets.

is the distance covered by the radiation in the planetary atmosphere given by (Tinetti et al., 2013):

$$l(z) = \int dl = \sqrt{(R_p + z_{max})^2 - (R_p + z)^2} \quad (13)$$

where R_p is the radius of the planet, below which the medium becomes opaque at all wavelength and z_{max} is the maximum height (on the top of R_p), above which photons do not suffer any absorption or scattering. We calculated the transmission spectra by using `Exo-Transmit` package (Kemp-ton et al., 2017). Figure 15 shows the transmission spectra for the present and the prebiotic Earth-like exoplanets. Figure 15a presents the transmission spectra up to a wavelength of $4.5 \mu\text{m}$ while Figure 15b shows the same up to the wavelength $30 \mu\text{m}$. The transmission depth due to absorption by O_2 , H_2O , CO_2 and O_3 are marked in the spectra. For the early or prebiotic Earth-like exoplanets, the absorption lines of only CO_2 molecules are seen.

In the transmission spectra of prebiotic Earth-like exoplanets presented in Figure 15(a), which is the zoomed-in version of Figure 15(b), signatures of CO_2 can be found at $1.4 \mu\text{m}$, $1.6 \mu\text{m}$, $2.0 \mu\text{m}$, $2.7 \mu\text{m}$ and at $4.3 \mu\text{m}$. On the other hand, the signatures of H_2O at $0.72 \mu\text{m}$, $0.82 \mu\text{m}$, $0.94 \mu\text{m}$, $1.10 \mu\text{m}$, $1.87 \mu\text{m}$ and $2.70 \mu\text{m}$ are clear in the transmission spectra of mod-

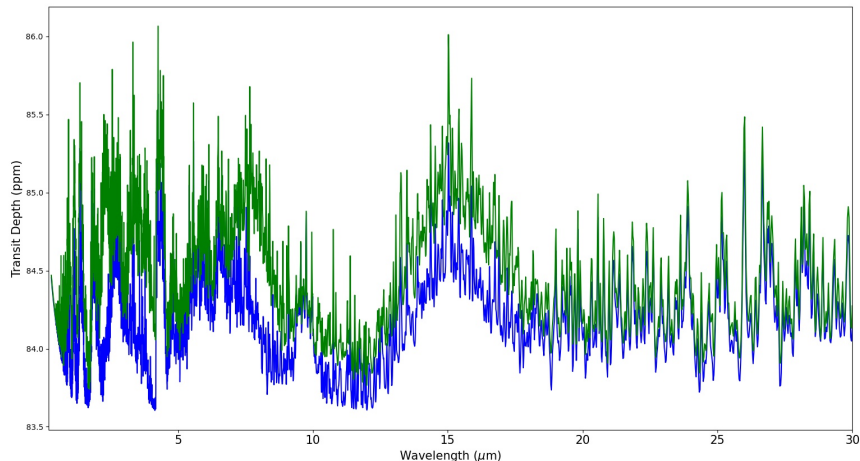


Figure 16: Transmission spectra of the present Earth but with increased greenhouse gas abundance (green). For a comparison, transmission spectrum (blue) of the Earth with actual atmospheric abundance is also presented.

ern Earth. In the transmission spectra of modern Earth, signatures of O_2 can also be found at $0.63 \mu\text{m}$, $0.69 \mu\text{m}$, $0.76 \mu\text{m}$ and that of CO_2 at $1.4 \mu\text{m}$, $2.7 \mu\text{m}$, $4.3 \mu\text{m}$. The signature of O_3 is visible at $3.3 \mu\text{m}$. Figure 15(b) shows the transmission spectra for the whole wavelength region i.e. $0.3 \mu\text{m}$ to $30.0 \mu\text{m}$.

Figure 16 shows the transmission spectra for the increased abundance of greenhouse gases in the atmosphere of the terrestrial exoplanet. Here we notice that the transmission depth increases with the increase in the abundance of greenhouse gases in the planetary atmosphere. However, this increase in the transmission depth is found to be confined only up to a certain wavelength region, which is again due to Rayleigh scattering.

3.3.2. Effects of cloud opacity

The observations of the various exoplanetary atmospheres indicate that the presence of clouds or hazes are common phenomenon in the planetary atmospheres (Kreidberg et al., 2014; Sing et al., 2016). This is one of the reasons for weak or no molecular feature observed in the transmission spectra of quite a few hot Jupiters (Sánchez-López et al., 2020). The same situation may arise for the terrestrial exoplanets if the upper atmosphere is covered

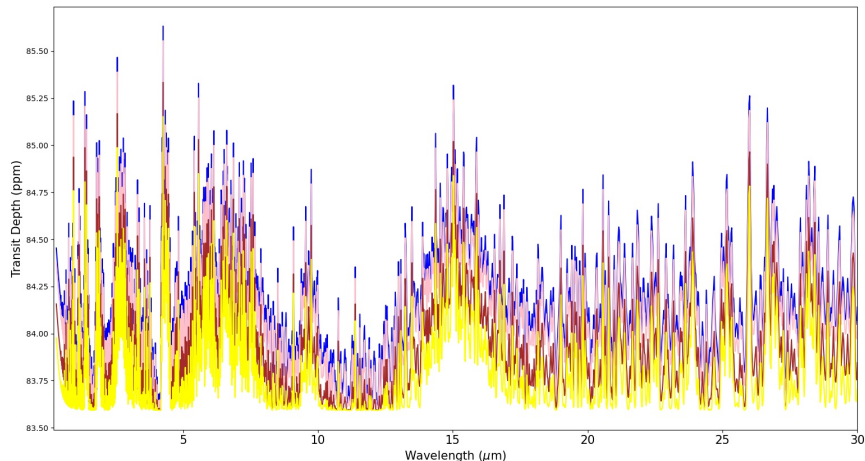


Figure 17: Transit spectra for present Earth with clear sky (blue) and for 100 percent cloud coverage at three different heights i.e. 2.2 km (pink), 9.5 km (brown) and 17.0 km (yellow) from the surface of the planet.

by clouds or hazes. The presence of clouds or hazes however, increases the Rayleigh scattering.

For the gray cloud calculation, we selected a pressure layer in the atmosphere at which the cloud top is optically thick. We provided a threshold pressure within the pressure range of the T - P profile and performed the radiative transfer calculations for pressures below that of the cloud deck. We used `Exo-Transmit` package (Kempton et al., 2017) for the calculation of cloud optical depth. Figure 17 shows the transmission spectra for clear sky and for the sky with 100% coverage of clouds at three different atmospheric heights i.e. 2.2 km, 9.5 km and 17.0 km from the surface of the planet.

4. Conclusions and Discussion

In the first part of this paper, we presented the numerical models of reflection spectra (in visible) for both the present and prebiotic Earth-like exoplanets orbiting within the habitable zone of main sequence stars of F, G, K and M spectral types. We also presented the model reflected spectra for the known exoplanets, which are orbiting around the stars of G, K and M spectral types.

We found that the nature of the reflected spectra is similar to that of the incident stellar spectrum i.e., the reflected flux peaks in the optical waveband but decrease significantly at longer wavelengths. However, Rayleigh scattering in the planetary atmosphere makes the reflected spectra comparatively steeper. The geometric albedo also decreases with the increase in wavelength because of the same reason i.e. Rayleigh scattering. The amount of reflected flux for the planets orbiting M dwarfs is significantly less compared to the stars of F, G and K spectral types. This is because the input stellar spectra peaks in the infrared wavelength region where Rayleigh scattering is negligible. The absorption lines of the biosignatures like O_2 , H_2O , O_3 , etc. are dominant in the geometric albedo. Owing to the fact that prebiotic early Earth-like exoplanets have a greater percentage of greenhouse gas CO_2 , they scatter more radiation than the present Earth-like exoplanets do. A present Earth-like exoplanet with higher abundance of greenhouse gases also have greater albedo. We have also estimated the maximum possible values of Bond albedo for the known exoplanets and thus given a limit on Bond albedo for the planets to remain habitable.

We also investigated the effects of surface Bond albedo on the reflected spectra and geometric albedo for various solid and liquid surface composition. We considered several kinds of solid and liquid surfaces e.g., (1) present Earth-like surface composition, (2) early Earth-like surface composition, (3) 100% ocean cover, (4) 50% ocean and remaining with trees and grass and (5) 83% ocean and remaining with snow. The reflected flux and the geometric albedo increases with the increase in surface albedo. It is minimum for no surface albedo at all. The effect of the surface albedo becomes negligible for an atmosphere thick enough to obstruct the incident stellar radiation to reach the solid or liquid surface. Thus, surface composition plays a key role in determining the reflectivity of the planet. In the infrared region, the planetary surface with ocean, vegetation, desert etc. play important role in determining the reflected as well as the re-emitted thermal radiation. However we did not considered the re-emitted thermal radiation here.

In the second part of the work, we presented the transmission spectra for present and prebiotic Earth-like exoplanets. Since the transmission depth increases at the shorter wavelength due to scattering, an increase in the abundance of greenhouse gases yields into greater transmission depth. Also, the transmission depth reduces in magnitude with the increase in the height of the cloud level. Since the `Exo-Transmit` code does not incorporate diffused radiation by scattering, it just reduces the transmission depth. As the

height of the cloud increases, the threshold pressure decreases. As a consequence, a comparatively smaller atmospheric region above the clouds yields a featureless transmission spectra. Since we assume a vertically homogeneous atmospheric abundance, the spectral feature remain the same, but the magnitude will change, with the change in the cloud height.

In the future, since many big-budget missions are coming like Habitable Worlds Observatory (HWO), GMT, Thirty Meter Telescope (TMT), Extremely Large Telescope (ELT), etc., our models will play an important role in the habitability study of the Earth-like exoplanets. By knowing their reflectivity, Bond albedo and the transmission spectra, we would be able to know about the factors like planet's surface and atmospheric composition, atmospheric T - P profile, presence of clouds, greenhouse gases, etc., which play a key role in determining the habitable planet.

Acknowledgements

We acknowledge the referee José A. Caballero for giving insightful comments and the improvement in the presentation of the paper. We thank Sukrit Ranjan for kindly providing model spectra for prebiotic Earth orbiting solar type of star and for many useful discussions. We also thank Adam Burgasser for providing the observed near infrared spectrum of TRAPPIST-1. MS would like to acknowledge Soumya Sengupta for fruitful discussions.

References

- Alonso, R., 2018. Characterization of Exoplanets: Secondary Eclipses. Springer International Publishing, Cham. pp. 1441–1467. URL: https://doi.org/10.1007/978-3-319-55333-7_40, doi:10.1007/978-3-319-55333-7_40.
- Alonso-Floriano, F., Morales, J., Caballero, J., Montes, D., Klutsch, A., Mundt, R., Cortés-Contreras, M., Ribas, I., Reiners, A., Amado, P., et al., 2015. Carmenes input catalogue of m dwarfs-i. low-resolution spectroscopy with cafos. *Astronomy & Astrophysics* 577, A128.
- Anglada-Escudé, G., Amado, P.J., Barnes, J., Berdiñas, Z.M., Butler, R.P., Coleman, G.A., de La Cueva, I., Dreizler, S., Endl, M., Giesers, B., et al., 2016. A terrestrial planet candidate in a temperate orbit around proxima centauri. *Nature* 536, 437–440. doi:<https://doi.org/10.1038/nature19106>.
- Armstrong, D., Pugh, C., Broomhall, A.M., Brown, D., Lund, M., Osborn, H., Pollacco, D., 2016. The host stars of kepler’s habitable exoplanets: superflares, rotation and activity. *Monthly Notices of the Royal Astronomical Society* 455, 3110–3125.
- Arney, G.N., 2019. The k dwarf advantage for biosignatures on directly imaged exoplanets. *The Astrophysical Journal Letters* 873, L7.
- Barbato, D., Bonomo, A., Sozzetti, A., Morbidelli, R., 2018. Revised estimates of the frequency of earth-like planets in the kepler field. arXiv preprint arXiv:1811.08249 .
- Batalha, N.E., Marley, M.S., Lewis, N.K., Fortney, J.J., 2019. Exoplanet reflected-light spectroscopy with picaso. *The Astrophysical Journal* 878, 70. doi:<https://doi.org/10.3847/1538-4357/ab1b51>.
- Bekker, A., Holland, H., Wang, P.L., Rumble, D., Stein, H., Hannah, J., Coetzee, L., Beukes, N., 2004. Dating the rise of atmospheric oxygen. *Nature* 427, 117–120.
- Borucki, W.J., Agol, E., Fressin, F., Kaltenegger, L., Rowe, J., Isaacson, H., Fischer, D., Batalha, N., Lissauer, J.J., Marcy, G.W., et al., 2013.

- Kepler-62: a five-planet system with planets of 1.4 and 1.6 earth radii in the habitable zone. *Science* 340, 587–590.
- Borucki, W.J., Koch, D.G., Batalha, N., Bryson, S.T., Rowe, J., Fressin, F., Torres, G., Caldwell, D.A., Christensen-Dalsgaard, J., Cochran, W.D., et al., 2012. Kepler-22b: A 2.4 earth-radius planet in the habitable zone of a sun-like star. *The Astrophysical Journal* 745, 120.
- Brocks, J.J., Logan, G.A., Buick, R., Summons, R.E., 1999. Archean molecular fossils and the early rise of eukaryotes. *Science* 285, 1033–1036.
- Bryson, S., Kunimoto, M., Kopparapu, R.K., Coughlin, J.L., Borucki, W.J., Koch, D., Aguirre, V.S., Allen, C., Barentsen, G., Batalha, N.M., et al., 2020. The occurrence of rocky habitable-zone planets around solar-like stars from kepler data. *The Astrophysical Journal* 161, 36. doi:<https://doi.org/10.3847/1538-3881/abc418>.
- Burgasser, A.J., Logsdon, S.E., Gagné, J., Bochanski, J.J., Faherty, J.K., West, A.A., Mamajek, E.E., Schmidt, S.J., Cruz, K.L., 2015. The brown dwarf kinematics project (bdkp). iv. radial velocities of 85 late-m and l dwarfs with mage. *The Astrophysical Journal Supplement Series* 220, 18.
- Burgasser, A.J., Mamajek, E.E., 2017. On the age of the trappist-1 system. *The Astrophysical Journal* 845, 110.
- Caballero, J., González-Álvarez, E., Brady, M., Trifonov, T., Ellis, T., Dorn, C., Cifuentes, C., Molaverdikhani, K., Bean, J., Boyajian, T., et al., 2022. A detailed analysis of the gl 486 planetary system. *Astronomy & Astrophysics* 665, A120.
- Chandrasekhar, S., 1960. Radiative transfer. Dover Publications, New York.
- Claudi, R., Alei, E., 2019. Biosignatures search in habitable planets. *Galaxies* 7, 82.
- Covone, G., Ienco, R.M., Cacciapuoti, L., Inno, L., 2021. Efficiency of the oxygenic photosynthesis on earth-like planets in the habitable zone. *Monthly Notices of the Royal Astronomical Society* 505, 3329–3335.
- Cuntz, M., Guinan, E., 2016. About exobiology: the case for dwarf k stars. *The Astrophysical Journal* 827, 79.

- Daylan, T., Pínglé, K., Wright, J., Günther, M.N., Stassun, K.G., Kane, S.R., Vanderburg, A., Jontof-Hutter, D., Rodriguez, J.E., Shporer, A., et al., 2021. Tess discovery of a super-earth and three sub-neptunes hosted by the bright, sun-like star hd 108236. *The Astronomical Journal* 161, 85.
- De Pater, I., Lissauer, J.J., 2015. *Planetary sciences*. Cambridge University Press.
- De Wit, J., Wakeford, H.R., Lewis, N.K., Delrez, L., Gillon, M., Selsis, F., Leconte, J., Demory, B.O., Bolmont, E., Bourrier, V., et al., 2018. Atmospheric reconnaissance of the habitable-zone earth-sized planets orbiting trappist-1. *Nature Astronomy* 2, 214–219.
- Domagal-Goldman, S.D., Segura, A., Claire, M.W., Robinson, T.D., Meadows, V.S., 2014. Abiotic ozone and oxygen in atmospheres similar to prebiotic earth. *The Astrophysical Journal* 792, 90.
- Dong, C., Lingam, M., Ma, Y., Cohen, O., 2017. Is proxima centauri b habitable? a study of atmospheric loss. *The Astrophysical Journal Letters* 837, L26.
- Ehrenreich, D., Tinetti, G., Des Etangs, A.L., Vidal-Madjar, A., Selsis, F., 2006. The transmission spectrum of earth-size transiting planets. *Astronomy and Astrophysics* 448, 379–393.
- Faucher, T.J., Turbet, M., Villanueva, G.L., Wolf, E.T., Arney, G., Kopparapu, R.K., Lincowski, A., Mandell, A., de Wit, J., Pidhorodetska, D., et al., 2019. Impact of clouds and hazes on the simulated jwst transmission spectra of habitable zone planets in the trappist-1 system. *The Astrophysical Journal* 887, 194.
- Faucher, T.J., Turbet, M., Wolf, E.T., Boutle, I., Way, M.J., Del Genio, A.D., Mayne, N.J., Tsigaridis, K., Kopparapu, R.K., Yang, J., et al., 2020. Trappist-1 habitable atmosphere intercomparison (thai): motivations and protocol version 1.0. *Geoscientific Model Development* 13, 707–716.
- Freedman, R.S., Lustig-Yaeger, J., Fortney, J.J., Lupu, R.E., Marley, M.S., Lodders, K., 2014. Gaseous mean opacities for giant planet and ultracool dwarf atmospheres over a range of metallicities and temperatures. *The Astrophysical Journal Supplement Series* 214, 25. doi:<https://doi.org/10.1088/0067-0049/214/2/25>.

- Freedman, R.S., Marley, M.S., Lodders, K., 2008. Line and mean opacities for ultracool dwarfs and extrasolar planets. *The Astrophysical Journal Supplement Series* 174, 504. doi:<https://doi.org/10.1086/521793>.
- Fujii, Y., Angerhausen, D., Deitrick, R., Domagal-Goldman, S., Grenfell, J.L., Hori, Y., Kane, S.R., Pallé, E., Rauer, H., Siegler, N., et al., 2018. Exoplanet biosignatures: observational prospects. *Astrobiology* 18, 739–778.
- Galuzzo, D., Cagnazzo, C., Berrilli, F., Fierli, F., Giovannelli, L., 2021. Three-dimensional climate simulations for the detectability of proxima centauri b. *The Astrophysical Journal* 909, 191.
- Garraffo, C., Drake, J.J., Cohen, O., 2016. The space weather of proxima centauri b. *The Astrophysical Journal Letters* 833, L4.
- Gilbert, E.A., Barclay, T., Schlieder, J.E., Quintana, E.V., Hord, B.J., Kostov, V.B., Lopez, E.D., Rowe, J.F., Hoffman, K., Walkowicz, L.M., et al., 2020. The first habitable-zone earth-sized planet from tess. i. validation of the toi-700 system. *The Astronomical Journal* 160, 116.
- Gillon, M., Jehin, E., Lederer, S.M., Delrez, L., de Wit, J., Burdanov, A., Van Grootel, V., Burgasser, A.J., Triaud, A.H., Opitom, C., et al., 2016. Temperate earth-sized planets transiting a nearby ultracool dwarf star. *Nature* 533, 221–224.
- Gillon, M., Triaud, A.H., Demory, B.O., Jehin, E., Agol, E., Deck, K.M., Lederer, S.M., De Wit, J., Burdanov, A., Ingalls, J.G., et al., 2017. Seven temperate terrestrial planets around the nearby ultracool dwarf star trappist-1. *Nature* 542, 456–460. doi:<https://doi.org/10.1038/nature21360>.
- Grenfell, J.L., Gebauer, S., Paris, P.v., Godolt, M., Rauer, H., 2014. Sensitivity of biosignatures on earth-like planets orbiting in the habitable zone of cool m-dwarf stars to varying stellar uv radiation and surface biomass emissions. *Planetary and Space Science* 98, 66–76.
- Grenfell, J.L., Stracke, B., von Paris, P., Patzer, B., Titz, R., Segura, A., Rauer, H., 2007. The response of atmospheric chemistry on earthlike planets around f, g and k stars to small variations in orbital distance. *Planetary and Space Science* 55, 661–671.

- Guo, Q., Strauss, H., Kaufman, A.J., Schröder, S., Gutzmer, J., Wing, B., Baker, M.A., Bekker, A., Jin, Q., Kim, S.T., et al., 2009. Reconstructing earth's surface oxidation across the archean-proterozoic transition. *Geology* 37, 399–402.
- Gvalani, S., 2022. A questionnaire-based study to understand knowledge and create awareness on the exoplanet-kepler 1649c. *The International Journal of Engineering and Science* .
- Hart, M.H., 1979. Habitable zones about main sequence stars. *ICARUS* 37, 351–357.
- Henry, T.J., Jao, W.C., Subasavage, J.P., Beaulieu, T.D., Ianna, P.A., Costa, E., Méndez, R.A., 2006. The solar neighborhood. xvii. parallax results from the ctiopti 0.9 m program: 20 new members of the recons 10 parsec sample. *The Astronomical Journal* 132, 2360.
- Hiatt, E.E., Pufahl, P.K., da Silva, L.G., 2020. Iron and phosphorus biochemical systems and the cryogenian-ediacaran transition, jacadigo basin, brazil: Implications for the neoproterozoic oxygenation event. *Precambrian Research* 337, 105533.
- Hill, M.L., Bott, K., Dalba, P.A., Fetherolf, T., Kane, S.R., Kopparapu, R., Li, Z., Ostberg, C., 2022. A catalog of habitable zone exoplanets. arXiv preprint arXiv:2210.02484 .
- Holland, H.D., 2002. Volcanic gases, black smokers, and the great oxidation event. *Geochimica et Cosmochimica acta* 66, 3811–3826.
- Hori, Y., Ogihara, M., 2020. Do the trappist-1 planets have hydrogen-rich atmospheres? *The Astrophysical Journal* 889, 77.
- Huang, S.S., 1959. Occurrence of life in the universe. *American Scientist* 47, 397–402. URL: <https://www.jstor.org/stable/27827376>.
- Huang, S.S., 1960. Life outside the solar system. *Scientific American* 202, 55–63. URL: <https://www.jstor.org/stable/24940446>.
- Husser, T.O., Wende-von Berg, S., Dreizler, S., Homeier, D., Reiners, A., Barman, T., Hauschildt, P.H., 2013. A new extensive library of phoenix stellar atmospheres and synthetic spectra. *Astronomy and Astrophysics* 553, A6.

- Ityaksov, D., Linnartz, H., Ubachs, W., 2008. Deep-uv absorption and rayleigh scattering of carbon dioxide. *Chem. Phys. Lett.* 462, 31–34.
- Jurgenson, C., Fischer, D., McCracken, T., Sawyer, D., Szymkowiak, A., Davis, A., Muller, G., Santoro, F., 2016. Expres: a next generation rv spectrograph in the search for earth-like worlds, in: *Ground-based and Airborne Instrumentation for Astronomy VI*, SPIE. pp. 2051–2070.
- Kaltenegger, L., 2017. How to characterize habitable worlds and signs of life. *Annu. Rev. Astron. Astrophys.* 55, 433–485. doi:<https://doi.org/10.1146/annurev-astro-082214-122238>.
- Kaltenegger, L., Lin, Z., Rugheimer, S., 2020. Finding signs of life on transiting earthlike planets: High-resolution transmission spectra of earth through time around fgkm host stars. *The Astrophysical Journal* 904, 10.
- Kaltenegger, L., Pepper, J., Christodoulou, P., Stassun, K., Quinn, S., Burke, C., 2021. Around which stars can tess detect earth-like planets? the revised tess habitable zone catalog. *The Astronomical Journal* 161, 233.
- Kaltenegger, L., Sasselov, D., Rugheimer, S., 2013. Water-planets in the habitable zone: atmospheric chemistry, observable features, and the case of kepler-62e and-62f. *The Astrophysical Journal Letters* 775, L47.
- Kaltenegger, L., Traub, W.A., 2009. Transits of earth-like planets. *The Astrophysical Journal* 698, 519. doi:<https://doi.org/10.1088/0004-637X/698/1/519>.
- Kaltenegger, L., Traub, W.A., Jucks, K.W., 2007. Spectral evolution of an earth-like planet. *The Astrophysical Journal* 658, 598.
- Kane, S.R., Hill, M.L., Kasting, J.F., Kopparapu, R.K., Quintana, E.V., Barclay, T., Batalha, N.M., Borucki, W.J., Ciardi, D.R., Haghhighipour, N., et al., 2016. A catalog of kepler habitable zone exoplanet candidates. *The Astrophysical Journal* 830, 1.
- Kane, S.R., Li, Z., Wolf, E.T., Ostberg, C., Hill, M.L., 2020. Eccentricity driven climate effects in the kepler-1649 system. *The Astronomical Journal* 161, 31.

- Kasting, J.F., Whitmire, D.P., Reynolds, R.T., 1993. Habitable zones around main sequence stars. *ICARUS* 101, 108–128. doi:<https://doi.org/10.1006/icar.1993.1010>.
- Kawashima, Y., Rugheimer, S., 2019. Theoretical reflectance spectra of earth-like planets through their evolutions: Impact of clouds on the detectability of oxygen, water, and methane with future direct imaging missions. *The Astronomical Journal* 157, 213. doi:<https://doi.org/10.3847/1538-3881/ab14e3>.
- Kemmer, J., Dreizler, S., Kossakowski, D., Stock, S., Quirrenbach, A., Caballero, J., Amado, P., Collins, K., Espinoza, N., Herrero, E., et al., 2022. Discovery and mass measurement of the hot, transiting, earth-sized planet, *gj 3929 b*. *A&A* 659, A17.
- Kempton, E.M.R., Lupu, R., Owusu-Asare, A., Slough, P., Cale, B., 2017. Exo-transmit: An open-source code for calculating transmission spectra for exoplanet atmospheres of varied composition. *Publications of the Astronomical Society of the Pacific* 129, 044402. doi:<https://doi.org/10.1088/1538-3873/aa61ef>.
- Kitzmann, D., Patzer, A., von Paris, P., Godolt, M., Rauer, H., 2011a. Clouds in the atmospheres of extrasolar planets-ii. thermal emission spectra of earth-like planets influenced by low and high-level clouds. *Astronomy and Astrophysics* 531, A62.
- Kitzmann, D., Patzer, A., von Paris, P., Godolt, M., Rauer, H., 2011b. Clouds in the atmospheres of extrasolar planets-iii. impact of low and high-level clouds on the reflection spectra of earth-like planets. *Astronomy and Astrophysics* 534, A63.
- Kitzmann, D., Patzer, A., von Paris, P., Godolt, M., Stracke, B., Gebauer, S., Grenfell, J., Rauer, H., 2010a. Clouds in the atmospheres of extrasolar planets-i. climatic effects of multi-layered clouds for earth-like planets and implications for habitable zones. *Astronomy and Astrophysics* 511, A66.
- Kitzmann, D., Vasquez, M., Patzer, A., Schreier, F., Rauer, H., Trautmann, T., 2010b. Influence of clouds on the reflection spectra of earth-like extrasolar planets, in: *European Planetary Science Congress 2010*, p. 725.

- Kopparapu, R.K., Ramirez, R., Kasting, J.F., Eymet, V., Robinson, T.D., Mahadevan, S., Terrien, R.C., Domagal-Goldman, S., Meadows, V., Deshpande, R., 2013. Habitable zones around main-sequence stars: new estimates. *The Astrophysical Journal* 765, 131.
- Kopparapu, R.K., Wolf, E.T., Meadows, V.S., 2020. Characterizing exoplanet habitability. *Planetary Astrobiology* , 449.
- Kreidberg, L., Bean, J.L., Désert, J.M., Benneke, B., Deming, D., Stevenson, K.B., Seager, S., Berta-Thompson, Z., Seifahrt, A., Homeier, D., 2014. Clouds in the atmosphere of the super-earth exoplanet gj 1214b. *Nature* 505, 69–72.
- Kreidberg, L., Loeb, A., 2016. Prospects for characterizing the atmosphere of proxima centauri b. *The Astrophysical Journal Letters* 832, L12.
- Krissansen-Totton, J., Garland, R., Irwin, P., Catling, D.C., 2018. Detectability of biosignatures in anoxic atmospheres with the james webb space telescope: A trappist-1e case study. *The Astronomical Journal* 156, 114.
- Lin, Z., Kaltenegger, L., 2020. High-resolution reflection spectra for proxima b and trappist-1e models for elt observations. *Monthly Notices of the Royal Astronomical Society* 491, 2845–2854.
- Lin, Z., MacDonald, R.J., Kaltenegger, L., Wilson, D.J., 2021. Differentiating modern and prebiotic earth scenarios for trappist-1e: high-resolution transmission spectra and predictions for jwst. *Monthly Notices of the Royal Astronomical Society* 505, 3562–3578.
- Louis, C., Snellen, I., Mouillet, D., Pepe, F., Wildi, F., Astudillo-Defru, N., Beuzit, J.L., Bonfils, X., Cheetham, A., Conod, U., et al., 2017. Atmospheric characterization of proxima b by coupling the sphere high-contrast imager to the espresso spectrograph. *Astronomy & Astrophysics* 599, A16.
- Luger, R., Lustig-Yaeger, J., Fleming, D.P., Tilley, M.A., Agol, E., Meadows, V.S., Deitrick, R., Barnes, R., 2017. The pale green dot: a method to characterize proxima centauri b using exo-aurorae. *The Astrophysical Journal* 837, 63.

- Lupu, R., Zahnle, K., Marley, M.S., Schaefer, L., Fegley, B., Morley, C., Cahoy, K., Freedman, R., Fortney, J.J., 2014. The atmospheres of earthlike planets after giant impact events. *The Astrophysical Journal* 784, 27. doi:<https://doi.org/10.1088/0004-637X/784/1/27>.
- Lustig-Yaeger, J., Meadows, V.S., Lincowski, A.P., 2019. The detectability and characterization of the trappist-1 exoplanet atmospheres with jwst. *The Astronomical Journal* 158, 27.
- Marley, M.S., Sengupta, S., 2011. Probing the physical properties of directly imaged gas giant exoplanets through polarization. *Monthly Notices of the Royal Astronomical Society* 417, 2874–2881. doi:<https://doi.org/10.1111/j.1365-2966.2011.19448.x>.
- Martinez-Rodriguez, H., Caballero, J.A., Cifuentes, C., Piro, A.L., Barnes, R., 2019. Exomoons in the habitable zones of m dwarfs. *The Astrophysical Journal* 887, 261.
- May, E., Taylor, J., Komacek, T., Line, M., Parmentier, V., 2021. Water ice cloud variability and multi-epoch transmission spectra of trappist-1e. *The Astrophysical Journal Letters* 911, L30.
- Mayor, M., Queloz, D., 1995. A jupiter-mass companion to a solar-type star. *Nature* 378, 355–359. doi:<https://doi.org/10.1038/378355a0>.
- Meadows, V., Arney, G., Schwieterman, E., Lustig-Yaeger, J., Lincowski, A., Robinson, T., Domagal-Goldman, S., Barnes, R., Fleming, D., Deitrick, R., Luger, R., Driscoll, P., Quinn, T., Crisp, D., 2016. The habitability of proxima centauri b: ii: Environmental states and observational discriminants. *Astrobiology* 18. doi:10.1089/ast.2016.1589.
- Meadows, V.S., Arney, G.N., Schwieterman, E.W., Lustig-Yaeger, J., Lincowski, A.P., Robinson, T., Domagal-Goldman, S.D., Deitrick, R., Barnes, R.K., Fleming, D.P., et al., 2018. The habitability of proxima centauri b: environmental states and observational discriminants. *Astrobiology* 18, 133–189. doi:<http://doi.org/10.1089/ast.2016.1589>.
- Mollière, P., Wardenier, J., van Boekel, R., Henning, T., Molaverdikhani, K., Snellen, I., 2019. petitradtrans-a python radiative transfer package for exoplanet characterization and retrieval. *Astronomy and Astrophysics* 627, A67.

- Moran, S.E., Hörst, S.M., Batalha, N.E., Lewis, N.K., Wakeford, H.R., 2018. Limits on clouds and hazes for the trappist-1 planets. *The Astronomical Journal* 156, 252.
- Morley, C.V., Fortney, J.J., Marley, M.S., Zahnle, K., Line, M., Kempton, E., Lewis, N., Cahoy, K., 2015. Thermal emission and reflected light spectra of super earths with flat transmission spectra. *The Astrophysical Journal* 815, 110.
- Neubauer, D., Vrtala, A., Leitner, J.J., Firneis, M.G., Hitzemberger, R., 2012. The life supporting zone of kepler-22b and the kepler planetary candidates: Koi268. 01, koi701. 03, koi854. 01 and koi1026. 01. *Planetary and Space Science* 73, 397–406.
- NOAA NASA US Air Force, 1976. US standard atmosphere, 1976. volume 76. National Oceanic and Atmospheric Administration.
- Och, L.M., Shields-Zhou, G.A., 2012. The neoproterozoic oxygenation event: Environmental perturbations and biogeochemical cycling. *Earth-Science Reviews* 110, 26–57.
- Owen, T., 1980. The search for early forms of life in other planetary systems: future possibilities afforded by spectroscopic techniques, in: *Strategies for the Search for Life in the Universe*. Springer, pp. 177–185.
- O'Malley-James, J.T., Kaltenegger, L., 2019. Lessons from early earth: Uv surface radiation should not limit the habitability of active m star systems. *Monthly Notices of the Royal Astronomical Society* 485, 5598–5603.
- Pallé, E., Muñoz, A.G., Osorio, M.R.Z., Montañés-Rodríguez, P., Barrena, R., Martín, E.L., 2010. Observations and modelling of earth's transmission spectrum through lunar eclipses: A window to transiting exoplanet characterization. *Proc Int Astron Union* 6, 385–388.
- Pallé, E., Osorio, M.R.Z., Barrena, R., Montañés-Rodríguez, P., Martín, E.L., 2009. Earth's transmission spectrum from lunar eclipse observations. *Nature* 459, 814–816.
- Peraiah, A., 2001. *An Introduction to Radiative Transfer*, by Annamaneni Peraiah. Cambridge, UK: Cambridge University Press.

- Peraiah, A., 2002. An Introduction to Radiative Transfer: Methods and applications in astrophysics. Cambridge University Press.
- Peraiah, A., Grant, I., 1973. Numerical solution of the radiative transfer equation in spherical shells. *J. Int. Math. Appl* 12, 75–90. doi:<https://doi.org/10.1093/imamat/12.1.75>.
- Perryman, M., 2018. The exoplanet handbook. Cambridge university press.
- Pickles, A., 1998. A stellar spectral flux library: 1150–25000 Å. *Publications of the Astronomical Society of the Pacific* 110, 863. doi:<https://doi.org/10.1086/316197>.
- Pidhorodetska, D., Fauchez, T.J., Villanueva, G.L., Domagal-Goldman, S.D., Kopparapu, R.K., 2020. Detectability of molecular signatures on trappist-1e through transmission spectroscopy simulated for future space-based observatories. *The Astrophysical Journal Letters* 898, L33.
- Quanz, S.P., Absil, O., Benz, W., Bonfils, X., Berger, J.P., Defrère, D., van Dishoeck, E., Ehrenreich, D., Fortney, J., Glauser, A., et al., 2021. Atmospheric characterization of terrestrial exoplanets in the mid-infrared: biosignatures, habitability, and diversity. *Experimental Astronomy* , 1–25doi:<https://doi.org/10.1007/s10686-021-09791-z>.
- Reylé, C., Jardine, K., Fouqué, P., Caballero, J.A., Smart, R.L., Sozzetti, A., 2021. The 10 parsec sample in the gaia era. *Astronomy & Astrophysics* 650, A201.
- Ribas, I., Gregg, M.D., Boyajian, T.S., Bolmont, E., 2017. The full spectral radiative properties of proxima centauri. *Astronomy and Astrophysics* 603, A58.
- Rodriguez, J.E., Vanderburg, A., Zieba, S., Kreidberg, L., Morley, C.V., Eastman, J.D., Kane, S.R., Spencer, A., Quinn, S.N., Cloutier, R., et al., 2020. The first habitable-zone earth-sized planet from tess. ii. spitzer confirms toi-700 d. *The Astronomical Journal* 160, 117.
- Rodríguez-Mozos, J., Moya, A., 2017. Statistical-likelihood exo-planetary habitability index (sephi). *Monthly Notices of the Royal Astronomical Society* 471, 4628–4636.

- Rugheimer, S., Kaltenegger, L., 2018. Spectra of earth-like planets through geological evolution around fgkm stars. *The Astrophysical Journal* 854, 19.
- Rugheimer, S., Kaltenegger, L., Zsom, A., Segura, A., Sasselov, D., 2013. Spectral fingerprints of earth-like planets around fgk stars. *Astrobiology* 13, 251–269.
- Rugheimer, S., Segura, A., Kaltenegger, L., Sasselov, D., 2015. Uv surface environment of earth-like planets orbiting fgkm stars through geological evolution. *The Astrophysical Journal* 806, 137. doi:<https://doi.org/10.1088/0004-637X/806/1/137>.
- Sabotta, S., Schlecker, M., Chaturvedi, P., Guenther, E., Rodríguez, I.M., Sánchez, J., Caballero, J., Shan, Y., Reffert, S., Ribas, I., et al., 2021. The carmenes search for exoplanets around m dwarfs–planet occurrence rates from a subsample of 71 stars. arXiv preprint arXiv:2107.03802 .
- Sagan, C., Thompson, W.R., Carlson, R., Gurnett, D., Hord, C., 1993. A search for life on earth from the galileo spacecraft. *Nature* 365, 715–721. doi:<https://doi.org/10.1038/365715a0>.
- Sánchez-López, A., López-Puertas, M., Snellen, I.A., Nagel, E., Bauer, F., Pallé, E., Tal-Or, L., Amado, P.J., Caballero, J., Czesla, S., et al., 2020. Discriminating between hazy and clear hot-jupiter atmospheres with carmenes. *Astronomy & Astrophysics* 643, A24.
- Sanz-Forcada, J., Micela, G., Ribas, I., Pollock, A.M., Eiroa, C., Velasco, A., Solano, E., García-Álvarez, D., 2011. Estimation of the xuv radiation onto close planets and their evaporation. *Astronomy & Astrophysics* 532, A6.
- Scharf, C., 2009. *Extrasolar planets and astrobiology*. University Science Books, Sausalito, Calif.
- Scheucher, M., Herbst, K., Schmidt, V., Grenfell, J.L., Schreier, F., Banjac, S., Heber, B., Rauer, H., Sinnhuber, M., 2020. Proxima centauri b: A strong case for including cosmic-ray-induced chemistry in atmospheric biosignature studies. *The Astrophysical Journal* 893, 12.
- Seager, S., 2010. *Exoplanet atmospheres : physical processes*. Princeton University Press, Princeton, N.J.

- Segura, A., Kasting, J.F., Meadows, V., Cohen, M., Scalo, J., Crisp, D., Butler, R.A., Tinetti, G., 2005. Biosignatures from earth-like planets around m dwarfs. *Astrobiology* 5, 706–725.
- Segura, A., Krelove, K., Kasting, J.F., Sommerlatt, D., Meadows, V., Crisp, D., Cohen, M., Mlawer, E., 2003. Ozone concentrations and ultraviolet fluxes on earth-like planets around other stars. *Astrobiology* 3, 689–708.
- Selsis, F., 2000. Physics of planets i: Darwin and the atmospheres of terrestrial planets, in: *Darwin and Astronomy: the Infrared Space Interferometer*, p. 133.
- Selsis, F., 2004. Atmospheric biomarkers on terrestrial exoplanets. *Boletin SEA* 12, 27–38.
- Selsis, F., 2004. The Atmosphere of Terrestrial Exoplanets: Detection and Characterization, in: Beaulieu, J., Lecavelier Des Etangs, A., Terquem, C. (Eds.), *Extrasolar Planets: Today and Tomorrow*, p. 170.
- Selsis, F., Kaltenegger, L., Paillet, J., 2008. Terrestrial exoplanets: diversity, habitability and characterization. *Physica Scripta* 2008, 014032.
- Sengupta, S., 2016a. Polarimetric detection of exoplanets transiting t and l brown dwarfs. *The Astronomical Journal* 152, 98. doi:<https://doi.org/10.3847/0004-6256/152/4/98>.
- Sengupta, S., 2016b. An upper limit on the ratio between the extreme ultraviolet and the bolometric luminosities of stars hosting habitable planets. *Journal of Astrophysics and Astronomy* 37, 1–11.
- Sengupta, S., 2018. Polarization of trappist-1 by the transit of its planets. *The Astrophysical Journal* 861, 41. doi:<https://doi.org/10.3847/1538-4357/aac6da>.
- Sengupta, S., Chakrabarty, A., Tinetti, G., 2020. Optical transmission spectra of hot jupiters: effects of scattering. *The Astrophysical Journal* 889, 181. doi:<https://doi.org/10.3847/1538-4357/ab6592>.
- Sengupta, S., Marley, M.S., 2009. Multiple scattering polarization of substellar-mass objects: T dwarfs. *The Astrophysical Journal* 707, 716. doi:<https://doi.org/10.1088/0004-637X/707/1/716>.

- Sengupta, S., Marley, M.S., 2010. Observed polarization of brown dwarfs suggests low surface gravity. *The Astrophysical Journal Letters* 722, L142. doi:<https://doi.org/10.1088/2041-8205/722/2/L142>.
- Sengupta, S., Marley, M.S., 2016. Detecting exomoons around self-luminous giant exoplanets through polarization. *The Astrophysical Journal* 824, 76. doi:<https://doi.org/10.3847/0004-637X/824/2/76>.
- Shields, A.L., Ballard, S., Johnson, J.A., 2016. The habitability of planets orbiting m-dwarf stars. *Phys. Rep.* 663, 1–38.
- Shields-Zhou, G., Och, L., 2011. The case for a neoproterozoic oxygenation event: geochemical evidence and biological consequences. *GSa Today* 21, 4–11.
- Sing, D.K., Fortney, J.J., Nikolov, N., Wakeford, H.R., Kataria, T., Evans, T.M., Aigrain, S., Ballester, G.E., Burrows, A.S., Deming, D., et al., 2016. A continuum from clear to cloudy hot-jupiter exoplanets without primordial water depletion. *Nature* 529, 59–62.
- Suissa, G., Wolf, E.T., kumar Kopparapu, R., Villanueva, G.L., Fauchez, T., Mandell, A.M., Arney, G., Gilbert, E.A., Schlieder, J.E., Barclay, T., et al., 2020. The first habitable-zone earth-sized planet from tess. iii. climate states and characterization prospects for toi-700 d. *The Astronomical Journal* 160, 118.
- Teegarden, B., Pravdo, S., Hicks, M., Lawrence, K., Shaklan, S., Covey, K., Fraser, O., Hawley, S., McGlynn, T., Reid, I., 2003. Discovery of a new nearby star. *The Astrophysical Journal* 589, L51.
- Tinetti, G., Encrenaz, T., Coustenis, A., 2013. Spectroscopy of planetary atmospheres in our galaxy. *The Astronomy and Astrophysics Review* 21, 63. doi:[10.1007/s00159-013-0063-6](https://doi.org/10.1007/s00159-013-0063-6).
- Torres, G., Kipping, D.M., Fressin, F., Caldwell, D.A., Twicken, J.D., Ballard, S., Batalha, N.M., Bryson, S.T., Ciardi, D.R., Henze, C.E., et al., 2015. Validation of 12 small kepler transiting planets in the habitable zone. *The Astrophysical Journal* 800, 99.

- Turbet, M., Bolmont, E., Bourrier, V., Demory, B.O., Leconte, J., Owen, J., Wolf, E.T., 2020. A review of possible planetary atmospheres in the trappist-1 system. *Space science reviews* 216, 1–48.
- Turbet, M., Leconte, J., Selsis, F., Bolmont, E., Forget, F., Ribas, I., Raymond, S.N., Anglada-Escudé, G., 2016. The habitability of proxima centauri b-ii. possible climates and observability. *Astronomy and Astrophysics* 596, A112.
- Vanderburg, A., Rowden, P., Bryson, S., Coughlin, J., Batalha, N., Collins, K.A., Latham, D.W., Mullally, S.E., Colón, K.D., Henze, C., et al., 2020. A habitable-zone earth-sized planet rescued from false positive status. *The Astrophysical Journal Letters* 893, L27.
- Waldmann, I.P., Tinetti, G., Rocchetto, M., Barton, E.J., Yurchenko, S.N., Tennyson, J., 2015. Tau-rex i: A next generation retrieval code for exoplanetary atmospheres. *The Astrophysical Journal* 802, 107.
- Wandel, A., Tal-Or, L., 2019. On the habitability of teegarden’s star planets. *The Astrophysical Journal Letters* 880, L21.
- Whitmire, D., Reynolds, R., Kasting, J., 1991. Habitable zones for earth-like planets around main sequence stars, in: *Bioastronomy*. Springer, pp. 173–178. doi:https://doi.org/10.1007/3-540-54752-5_210.
- Wildi, F., Blind, N., Reshetov, V., Hernandez, O., Genolet, L., Conod, U., Sordet, M., Segovilla, A., Rasilla, J., Brousseau, D., et al., 2017. Nirps: an adaptive-optics assisted radial velocity spectrograph to chase exoplanets around m-stars, in: *Techniques and Instrumentation for Detection of Exoplanets VIII*, SPIE. pp. 321–335.
- Wolf, E.T., 2017. Assessing the habitability of the trappist-1 system using a 3d climate model. *The Astrophysical Journal Letters* 839, L1.
- Wolf, E.T., 2018. Erratum: “assessing the habitability of the trappist-1 system using a 3d climate model” (2017, *apjl*, 839, 11). *The Astrophysical Journal Letters* 855.
- Wunderlich, F., Godolt, M., Grenfell, J.L., Städt, S., Smith, A.M., Gebauer, S., Schreier, F., Hedelt, P., Rauer, H., 2019. Detectability of atmospheric

- features of earth-like planets in the habitable zone around m dwarfs. *Astronomy and Astrophysics* 624, A49.
- Wunderlich, F., Scheucher, M., Godolt, M., Grenfell, J.L., Schreier, F., Schneider, P.C., Wilson, D.J., Sánchez-López, A., López-Puertas, M., Rauer, H., 2020. Distinguishing between wet and dry atmospheres of trappist-1 e and f. *The Astrophysical Journal* 901, 126.
- Yan, F., Fosbury, R.A., Petr-Gotzens, M.G., Zhao, G., Wang, W., Wang, L., Liu, Y., Pallé, E., 2015. High-resolution transmission spectrum of the earth's atmosphere-seeing earth as an exoplanet using a lunar eclipse. *Int. J. Astrobiology* 14, 255–266.
- Zechmeister, M., Dreizler, S., Ribas, I., Reiners, A., Caballero, J., Bauer, F., Béjar, V., González-Cuesta, L., Herrero, E., Lalitha, S., et al., 2019. The carmenes search for exoplanets around m dwarfs-two temperate earth-mass planet candidates around teegarden's star. *Astronomy & Astrophysics* 627, A49.
- Zhang, Z., Zhou, Y., Rackham, B.V., Apai, D., 2018. The near-infrared transmission spectra of trappist-1 planets b, c, d, e, f, and g and stellar contamination in multi-epoch transit spectra. *The Astronomical Journal* 156, 178.